CR-111883

EFFECT OF STRAIN RATE AND LOAD CYCLING ON THE TENSILE BEHAVIOR AND AIR PERMEABILITY OF A COATED FABRIC

Contract No. NAS 1-9816

EFFECT OF STRAIN RATE AND LOAD CYCLING ON THE TENSILE BEHAVIOR AND AIR PERMEABILITY OF A COATED FABRIC

by

J. Skelton and N. J. Abbott

Prepared under Contract No. NAS 1-9816 by
FABRIC RESEARCH LABORATORIES, INC.
Dedham, Mass.

for

NATIONAL AERONAUTICS AND SPACE ADMINISTRATION

EFFECT OF STRAIN RATE AND LOAD CYCLING ON THE TENSILE BEHAVIOR AND AIR PERMEABILITY OF A COATED FABRIC

By J. Skelton and N. J. Abbott

ABSTRACT

The tensile behavior and air permeability of a lightweight Viton-coated Nomex fabric were determined after exposure to various levels of cyclic stress applied at a range of strain rates. Specimens were stressed uniaxially to failure, and also to 25%, 50% and 75% of their failure load for one and ten cycles of stress, at strain rates of 1, 10, 100, 1000 and 10,000%/sec; specimens were stressed biaxially at approximately 1%/sec to similar load levels. The uniaxial tensile behavior was shown to be relatively insensitive to strain rate. The air permeability of the fabric was very low under all conditions of prestress and measurement load. This result is in contrast to the data presented in NASA TN D-5931 for a similar coated fabric. It is suggested that the difference between the two fabrics is related to a critical level of coating material add-on. This level is the amount of coating required to fill all the interstices and to provide, in addition, a continuous coherent layer over the fabric surface.

INTRODUCTION

Studies of the dynamics of entry into low-density atmospheres have demonstrated the need for the development of decelerator systems capable of performing efficiently at high supersonic speeds. Current parachute concepts are not suitable under these conditions since the high geometric porosity required to give good stability result in low drag coefficients (ref. 1). One system currently under consideration is the Attached Inflatable Decelerator (AID), which is a low mass, inflatable canopy attached directly to the payload, such that on deployment the frontal area of the payload is considerably increased with a corresponding increase in drag coefficient (ref. 2).

The design requirements for the canopy material of low mass and packed volume and high strength and flexibility are well met by textile fabrics. Studies of models of an AID configuration specifically designed for entry into low density atmospheres have shown that the fabric on the rear surface of the AID must be of very low permeability in order to achieve the large frontal area of the design shape (ref. 3). The required low values of permeability can only be achieved by coating the fabric in order to fill the inter-yarn interstices. Since supersonic deceleration at high Mach numbers may cause severe aerodynamic heating of the decelerator, it is important that the canopy fabric be thermally durable. The currently favored material is a light plain weave Nomex fabric, coated with Viton.

In addition to the air permeability, the tensile behavior of the canopy fabric is an important factor controlling the design and performance of the AID, and rational design procedures can be followed only if these data are available. During deployment the canopy is subjected to high-strain rate biaxial loading, followed by a relatively steady load during the active phase. Throughout the load history, however, the fabric may be subjected to high strain rate oscillatory stress as a result of flutter or other local instabilities. The most valid design data for the canopy fabric will be those obtained under stress conditions similar to those experienced by the canopy under flight conditions. Since both the polymer used in the base fabric, and the Viton coating are viscoelastic it is to be expected that the behavior of the coated fabric will be dependent on its previous strain history, and there is evidence (ref. 4) that the air permeability of lightweight coated fabrics can be greatly increased under certain loading conditions. The current report gives results of a test program designed to determine the effect of strain rate, load cycling and stress level on the air permeability and the tensile behavior of the canopy fabric. In view of the experimental difficulties involved in carrying out biaxial tensile tests at high strain rates, the major part of this investigation was concerned with uniaxial loading. However some biaxial loading conditions were investigated at low strain rates in order to provide some measure of correlation between the two stress modes.

DETAILS OF COATED FABRIC

The fabric used in this investigation was similar to that which has been used in a variety of investigations at NASA Langley Research Center, including that described in reference 3. The fabric was 2.4 ozm/yd^2 (0.08 kg/m^2) plain weave, woven from 100 denier (11 Tex) Nomex yarn. Approximately 130 yards (119m) of fabric in the scoured and heat-set state were received from NASA Langley and were subsequently calendered by Kenyon Piece Dye Works, Kenyon, Rhode Island. After calendering, the fabric was coated with Viton by the Duracote Corporation, Ravenna, Ohio. Following the removal of short samples at various stages to serve as reference materials, and inevitable processing loss, approximately 118 yards (108m) of usable coated fabric were available for testing.

Constructional details of the fabric in the various states are given in Table 1. The thickness of the fabric is reduced considerably by calendering, but is restored almost to its original value by coating. The ends and picks per unit length, and hence the weight per unit area, are increased slightly by calendering; subsequent coating does not change the ends and picks per unit length significantly, but adds 0.4 ozm/yd^2 (0.01 kg/m^2) to the mass. The air permeability is reduced by a factor of approximately 2.5 by the calendering process, and by a further factor of approximately 300 by the coating, which effectively seals up all the inter-yarn interstices. Figures 1(a) and 1(b) show sections along the warp and filling yarns respectively of the coated fabric, and Figures 2 and 3 show the surface features of the coated and uncoated sides respectively. The flattening of the individual filaments can be clearly seen, as can the distorted yarn paths; both these effects are results of the calendering. The coating is very thin on the surface of the fabric, and most of the coating material appears to be in the spaces between the filaments. Indeed, the increase in thickness noted on coating is caused principally by this penetration, rather than the deposition of a thick layer of coating material.

TEST PROCEDURES AND CONDITIONS

The general scheme of stress history and subsequent testing, to which all specimens were subjected, consisted of the application of cycles of stress up to a particular fraction of the breaking load, followed by the measurement of air permeability under a range of stress conditions. The cyclic loads were applied at strain rates of 1, 10, 100, 1,000, and 10,000 percent per second, for 1 and for 10 cycles of load. The maximum stress level during test cycling was 25%, 50% or 75% of the breaking load measured at the 1% per second strain rate. After load cycling the specimens were stressed to various load levels at approximately 1% per second strain rate, and the air permeability was measured. The load levels applied during this phase of the testing varied somewhat from specimen to specimen, but typical

values were 10%, 60% and 80% of the breaking load measured at the slowest strain rate. In addition to the air permeability measurements, tensile tests were carried out at the various strain rates on uncycled control specimens, and at 1% per second on specimens subjected to load cycling.

Load cycling and tensile tests at 1 and 10% per second were carried out using the Instron tensile tester with an 8.3 inch (21.1 cm) gauge length and 5 inch/minute (0.21 cm/s) and 50 inch/minute (2.1 cm/s) jaw speeds respectively. The load cycling cams of the Instron were set to cycle between zero load and 25, 50 and 75% of the breaking load measured at 1% per second. The load cycling tests were carried out on 3 inch (7.6 cm) wide specimens to allow for subsequent air permeability measurements, while the tensile tests were carried out on 1 inch (2.5 cm) wide ravelled strip specimens.

The Instron tensile tester cannot be used to provide strain values much in excess of 10% per second; the maximum strain rate is set by the maximum jaw speed (50 inches/minute; 2.1 cm/s) and the shortest practical gauge length (approximately 6 inches; 15.2 cm). It was originally intended to use the FRL® large Piston Tester for all strain rates greater than 10% per second. In fact, however, the FRL® tester proved to be very inconvenient and time consuming at 100% per second, and a drop-weight method was devised for stressing materials at this strain rate.

The design and operation of the FRL® Large Piston Tester is fully described in reference 5, but a brief description and specification will be repeated here. The specimen under test is mounted slack between an upper jaw which is suspended from a piezoelectric force gauge attached to a rigid frame, and a lower jaw carried by a piston that is driven by the release of compressed gas from an accumulator. The piston has a stroke of 5 ft (1.5m), of which approximately 2 ft (0.6m) are required for acceleration, and the remaining 3 ft (0.9m) are the working and deceleration stroke. The exact variation of piston speed over the full stroke depends on the maximum velocity and the tensile behavior of the test specimen, with a minimum working stroke of about 1 ft (0.3m); the maximum velocity attained is controlled by the gas pressure in the accumulator.

The position of the lower jaw, and hence the strain in the specimen, is deduced from the measurement of a magnetic tape with a pre-recorded signal of known frequency, pulled past a pick-up head by the movement of the piston. The load and piston signals are displayed on a Tektronix dual-beam oscilloscope, and are recorded with a Polaroid camera. The maximum design tensile load is approximately 1000 lbf (4450N), and the maximum speed is approximately 200 ft/s (61 m/s). An overall view of the equipment is shown in Figure 3.

In order to test over a wide range of strain rates it is necessary to vary both the gauge length and the piston velocity. The shortest available gauge length that can be tested is

2 ft (0.6m), and this, together with a maximum jaw speed of 200 ft/s (61m/s) gives the maximum available strain rate of 10,000 %/s. Various combinations of jaw speed and gauge length can be used to achieve a strain rate of 1000% per second; in the current series of tests 20 ft/s (6m/s) and a 2 ft (0.6m) gauge length were used. The minimum strain rate theoretically attainable is 100% per second, achieved with the minimum jaw speed of 10 ft/sec (3m/s) and a 10 ft (3m) gauge length, but as was previously described the tester was not used at this strain rate during this program.

Since the piston tester does not have the load cycling facility of the Instron tester an alternative means of limiting the load experienced by the specimen was devised. The main problem associated with load cycling on an instrument such as the piston tester is that the maximum load to which the specimen is subjected cannot be controlled by stopping the moving jaw, since the inertia of the moving system is too high to permit rapid deceleration. Several means of limiting the maximum load were tried. The method finally adopted involved the incorporation of a "weak link", in series with the specimen, which would break at the desired load. The simplest and most reliable version of this technique used a dumbbell shaped tail of the same fabric sewn in series with the test specimen, the narrowest part of the dumbbell being cut to 25%, 50%, or 75% of the full width of the specimen. Thus when the load rose to the decided upper limit, the tail broke and the load was immediately removed from the specimen. In order to cycle the specimen repeatedly, 10 such tails were sewn to the specimen as shown in Figure 4. These were gripped successively in the lower jaw and broken in sequence until 10 loading cycles were completed.

The method appeared to work very well. Uniform distribution of load in the test specimen above the dumbbell strip was assured by sewing a very stiff seam between the two components. The reproducibility of the results may be seen in Figure 5 which shows typical oscilloscope traces from four succssive load cycles to 75% of rupture load at 1000% per second for warp specimens. The lower curve in each case represents the build-up of load in the test specimen; in the four cases illustrated the maximum loads were 205, 205, 210 and 203 lbs, all very close to the calculated value of 204 lbs based on 75% of the breaking load of the material. The upper curve shows the signal from the magnetic tape pick-up head from which the strain rate in the specimen may be calculated. The magnetic tape in the tests was attached to the lower end of the specimen, and the jaw speed was adjusted during trial shots to give the proper strain rate within the specimen itself.

The load cycling at 100% per second was carried out using the same technique of load limitation, but the load was applied to the specimens by means of a falling weight. If a weight is attached to a specimen of length ℓ and is dropped from a height s it is apparent that in order to set up an initial strain rate of 100% per second within the specimen the following relationship must hold:

$$\ell^2 = 64s.$$

Thus for a four foot (1.2m) long specimen, the weight should fall 3 inches (7.6 cm) before applying load to the specimen. The experimental arrangement is shown in Figure 6. The test specimen, including the deliberate weak link, is sewn in parallel with a shorter strip of the same fabric which supports the weight. When the supporting fabric is cut, the weight falls a predetermined amount before breaking the weak link. The precise distance of fall was adjusted during each test series to give a measured strain rate of 100% per second in the specimen. Because of the non-uniform velocity of the weight during the straining of the specimens, which varies somewhat with the strength of the weak link, the strain rate was not as constant during this series of tests as in the tests at other strain rates. However, since previous work at 1, 10, 1,000, and 10,000% per second had shown that the behavior of the fabric was very insensitive to strain rate, this slight variation in rate was not considered to be significant.

Tensile tests at 100%, 1,000% and 10,000% per second were carried out on 1 inch (2.5 cm) ravelled strip specimens using the FRL® small piston tester. This is a small version of the tester previously described, and uses the same load and elongation measurement techniques (reference 6).

The biaxial load cycling and tensile testing were carried out using a biaxial tester in which a cruciform specimen is loaded through a mechanical linkage by a manually operated hydraulic pump (reference 7). Because of the unbalanced nature of the fabric and the varying load ratio in the two directions of stress a single value of strain rate can not be given for the biaxial tests; however, the strain rate fell within the range 1-10% per second for all specimens tested. The elongations in the two directions were measured from photographs of a grid marked in the center of the specimen.

The air permeability measurements under tensile load were carried out using a technique developed at FRL® for the measurement of fabrics with very low permeability. The equipment is shown in Figure 7; the specimen is clamped between two flat plates having a center hole of area exactly 0.020 ft^2 (18.6 cm^2). Compressed air is supplied through a pressure reducing valve and a flowmeter to a small reservoir in the bottom plate and thence flows through the fabric to the ambient air. The pressure can be regulated and held constant within the range 0-35 inches of water (0-8.7 KN/m^2) and the amount of flow can be measured to the nearest 0.001 ft^3 (28.3 cm^3). In the permeability measurements on the Viton coated Nomex fabric, the tensile loads, either uniaxial or biaxial, were applied by means of the loading device shown in Figure 8, which consists of four identical hydraulic cylinders equipped with wide jaws for holding the fabric. The air permeability of the control fabric was low for all conditions of test so that no meaningful measurement could be made at a pressure differential of 0.5 inch of water (124 N/m^2). Instead measurements were made at 5-10 inches of water (1.24-2.48 KN/m^2) and the values of permeability were corrected to 0.5 inch of water

(124 N/m^2), using linear proportionality between flow and pressure. This linear relationship is theoretically valid for impermeable sheet materials, and its validity was checked experimentally for the coated fabric.

All cycling and tensile tests with the exception of the load cycling at 100, 1,000 and 10,000% per second were carried out at 70±2°F and 65±2% RH; the cycling noted above was carried out at 70±4°F and an estimated range of 55-70% RH. In view of the complete penetration of the coating materials into the fabric, it is not thought that the deviation from standard moisture conditions could affect the fabric significantly.

TENSILE BEHAVIOR

Typical uniaxial load-elongation curves for the fabric at various strain rates are given in Figures 9 through 13. Results for breaking load and breaking elongation are given in Table 2 and the variation of these properties with strain rate is shown in Figure 14. At all strain rates the fabric has a higher modulus in the warp direction than in the filling direction; this is a consequence of the greater crimp in the filling direction, as demonstrated by the cross sections shown in Figure 1. The curves for the warp direction, in which the crimp is small, are in substantial agreement with the data for Nomex yarns reported in reference 8, and the results for both warp and filling direction show the expected increase in initial modulus with increasing strain rate. The variation of breaking load and breaking elongation with strain rate show some unexpected trends. Measurements on Nomex yarn showed no change in breaking load with strain rates over the range considered here, and showed evidence of a maximum in breaking elongation at approximately 10%/sec followed by a region in which the breaking elongation decreased with increasing strain rate. Finally, at approximately 10,000%/second the breaking elongation again increased. The results for fabric breaking elongation show a similar maximum at low strain rates, but the final increase at high strain rates is not present for the warp direction. The breaking load curves for thefabric also show a maximum at low strain rates. The response of a fabric to tensile load depends in a complex manner on the intrinsic polymer response and the geometrical configuration of the yarns, and the measured variation for the fabric presumably reflects the interactions of these influences. Perhaps the important aspect of the results for design purposes is that no serious degradation of fabric properties occurs at high strain rate.

The breaking loads and elongation measured at a strain rate of 1%/sec for specimens exposed to load-cycling at various strain rates are given in Tables 3 through 7. The breaking load and elongation of the warp specimens are essentially unaffected by the prestressing, with the exception that the prestressing at 100%/second appears to lead to an increase in breaking load and elongation, particularly for single cycles of prestress. In the filling direction the fabric is more sensitive to the effects of prestressing. Specific trends are

difficult to discern, but a typical loss of approximately 10% in breaking load is observed. The breaking elongation in the filling direction is also considerably reduced by prestressing, a 30% reduction being typical. This fall in breaking elongation in the filling direction is a further consequence of the higher crimp in the filling yarns which is irreversibly removed by prestressing, giving a residual breaking elongation similar to that found in the warp direction. In view of the severity of the prestressing schedule the degradation in fabric tensile behavior is remarkably small.

Typical biaxial load-elongation curves for the fabric for various ratios of (warp load/filling load) are shown in Figures 15 through 17. These figures are drawn to the same scale as Figures 9-13 to facilitate comparisons of tensile behavior. There is no satisfactory way of determining true breaking loads and elongations under biaxial load, and all the curves shown were terminated by tearing failure originating at the reentrant corners of the cruciform specimen.

Figure 15 shows the typical biaxial tensile behavior for a (warp load/filling load) ratio of 1:1. All the specimens tested under these conditions failed in the warp direction at a load level of approximately 67 lb/inch (11.7 kN/m). The curves are steeper than the corresponding curves under uniaxial loading. This is a consequence of the fact that the mechanism of crimp interchange is hindered under biaxial loading conditions. Since the curves are both steeper, and end at a lower load level, the elongations at failure are much lower than under uniaxial load.

The tensile behavior for a (warp load/filling load) ratio of 2:1 is shown in Figure 16. The specimens broke in the warp direction at approximately 70 lb/in (12.3 kN/m). Since the filling yarns are not under as great a tension as the warp yarns, the crimp interchange is not as severely hindered as it is under a 1:1 load ratio; consequently the warp curve is less steep and the filling curve steeper than the corresponding curves under a 1:1 load ratio.

Figure 17 shows the tensile behavior for a (warp load/filling load) ratio of 1:2. In this case, the greater load is on the filling yarns, which pull straight with relative ease and have a load elongation characteristic quite close to that found for uniaxial load. The warp yarns, however, which are under smaller load, become more crimped as the filling yarns straighten, and the fabric shows a contraction in the warp direction. This contraction is maintained up to load levels of approximately 30 lb/in (5.3 kN/m) at which point the increasing axial extension of the warp yarns balances the geometrical contraction. The specimen failed in the filling direction at approximately 80 lb/in (14.0 kN/m).

In summary, the biaxial tensile behavior is consistent with predictable principles. Any degree of elongation is achieved at the lowest load when the crosswise direction is free

from tension (uniaxial loading). That load increases as the load in the crosswise direction is increased. Thus, for example, the loads required for 5% elongation in each direction were as follows:

LOADS REQUIRED TO PRODUCE 5% ELONGATION UNDER VARIOUS STATES OF BIAXIAL LOAD

Crosswise Load/ Lengthwise Load	Warp Load, lb/in	Warp Load, (kN/m)	Filling Load, lb/in	Filling Load, (kN/m)
0	53	9.3	14	2.5
0.5	60	10.5	23	4.0
1.0	62	10.9	27	4.7
2.0	broke at 2% elongation due to filling failure		34	6.0

AIR PERMEABILITY

The air permeability values for the Viton-coated Nomex fabric after various cycles of uniaxial prestress at a range of strain rates are given in Tables 8-12 and the data are plotted in Figures 18-29. In each of these figures, Lp signifies the load level to which the specimens were cycled, and Lm the tension under which the specimen was held when the permeability was measured. Both of these loads are expressed as a percentage of the breaking load at 1%/sec strain rate. The air permeability values for the biaxially cycled fabrics are given in Table 13 and plotted in Figures 30-35. For comparison purposes, the permeability of uncycled fabric under various load conditions is given in Table 14.

Examination of the data reveals several interesting trends. Under all conditions of prestress, the absolute value of the air permeability remains very low, and the material is essentially impermeable to air. Nevertheless, all specimens show an increase in air permeability with increasing stress level during measurement, with the filling specimen generally showing a greater increase than the warp specimens under a given load. Since there is no evidence of coating breakdown, the measured increases in air permeability presumably reflect the decrease in thickness of the coating under stress; the filling specimens, with their lower modulus, are affected to a greater extent than the warp specimens at a given load level.

The air permeability at a given load level generally increases with increasing level of and number of cycles of prestress. The increase in permeability is greatest for specimens prestressed at low strain rates than at high strain rates. This type of behavior is contrary to the anticipated behavior, since it was expected that the possibility of different strain rate sensitivity

in the fabric and the coating material might lead to mismatches in elongation at high strain rates, with subsequent breakdown in the coating adhesion. In fact, the amount of increase in air permeability appears to be related to the total time spent under prestress conditions. This suggests that some irreversible creep is taking place in the coating material, leading to local thinning of the coating, and hence to an increase in permeability.

The specimens prestressed at high strain rates could not be held under a load of more than approximately 60% of the breaking load when stressed in the air permeability apparatus, while specimens stressed at low strain rates were able to sustain loads up to 80% of the breaking load of the fabric. Thus this aspect of the tensile behavior, which is controlled by the base fabric, contrasts with the air permeability behavior, which is controlled by the coating material. However, as was previously noted, the breaking load of the fabric measured under a standard set of conditions is not significantly affected by the prestress conditions.

The air permeability under biaxial load conditions is in general agreement with the trends to be anticipated on the basis of the biaxial tensile behavior. With (warp load/filling load) ratios of 1:1 and 1:2 the behavior is dominated by the influence of the more readily extensible filling direction; with a load ratio of 2:1 the behavior is predominantly influenced by the warp characteristics.

The air permeability behavior found for the Viton-coated Nomex fabric is in complete contrast with that described in reference 4 for a similar material. Since the air permeability is a critical parameter for the intended end-use some reason for this discrepency was sought. Samples of both fabrics were duplicate tested, using both the Gurley air permeometer as described in reference 4 and the air flow meter as described in this report. No difference was observed between the two methods of test, both indicating essentially zero permeability. However, during the course of the testing, specimens from particular areas of the original fabric were found to have the high permeability values previously reported. The only explanation for this type of behavior appears to be a real variability in the properties of the fabric, and a detailed examination of the physical properties of the fabrics suggests how such a variability might arise. The photomicrographs of the current fabric shown in Figure 1, and similar photomicrographs of the original fabric, show that almost all the coating material is held within the interstices of the base fabric.

The earlier fabric was made fron 100 denier (11 Tex) Nomex, woven 81x75 yarns per inch (32x30 yarns per cm). This exact fabric was unavailable for the present work. In its place, a fabric made from 100 denier (11 Tex) Nomex woven 83x93 yarns per inch (32.7x36.6 yarns per cm) was used. This fabric was obviously slightly heavier but, more importantly, more tightly woven than the earlier fabric. Both were coated with about 0.5 oz/yd^2 (0.02 kg/m^2) of Viton. It is likely that this was the minimum

amount needed to provide the desired low level of permeability in the lighter, more open fabric. That is to say, it is the amount required to fill the pores of the woven fabric, with only a slight excess on the surface as a film. Because the second fabric was more tightly woven, that is, its pores were smaller, and the amount of coating required to fill them was undoubtedly less than for the more open fabric, leaving a thicker film on the surface.

The discussion presented above indicates the possibility that the permeability of coated fabrics after load cycling might show a region of high sensitivity to the amount of coating material, centered on a particular coating weight at which the interstices were just filled. Under these conditions small changes in fabric construction or coating conditions would have a disproportionate effect on the behavior of the fabric, and large point to point variations in properties could occur. This possibility, suppored as it is by large range in measured air permeability values in the earlier fabric, makes clear the desirability for 100% inspection of fabric intended for use in such critical applications as AIDs. Alternatively, it may be more desirable to over-engineer the fabric and accept a small weight penalty in the form of slight excess coating material rather than risk the possibility of mechanical breakdown, particularly since the current work shows the extremely high dependability of the coating if integrity can be maintained. A study of the detailed variation of coating integrity under cyclic stress with coating weight for such lightweight fabrics would form a very useful extension of the present work.

CONCLUSIONS

The tensile behavior and air permeability, measured at a pressure differential of 0.5 in water (1240N/m^2) and converted to a pressure differential of 0.5 in water (124 N/m^2), were determined for a lightweight Viton coated Nomex fabric after exposure to various levels of cyclic stress applied at a range of strain rates. Specimens were stressed uniaxially to break, and also to 25%, 50% and 75% of their breaking load for one and for ten cycles of stress, at strain rates of 1, 10, 100, 1,000, and 10,000 percent per second, and biaxially to 25%, 50% and 65% of the breaking load with (warp load/filling load) ratios of 1:1, 2:1 and 1:2 at a strain rate of approximately 1% per second. The uniaxial tensile behavior of all the uniaxially stressed specimens was measured at a strain rate of 1% per second and the air permeability of all specimens was measured under various load conditions.

The uniaxial load-elongation behavior of the fabric is different in the warp and filling directions, as a result of the greater crimp in the filling yarns. The differences between the two directions, marked mainly by the greater elongation in the filling direction under a given load, persist at all strain rates and the general form of the curves are relatively insensitive to

strain rates. The end points of the curves show some strain rate sensitivity, with both the breaking loads and breaking elongations passing through maxima at approximately 100% per second. The biaxial behavior is consistent with the uniaxial data, both directions showing an increase in tensile modulus over the uniaxial values, as a result of the hindrance of the crimp interchange. The breaking loads and elongations are considerably reduced under biaxial loading conditions.

The air permeability of the fabric under zero load is very low, and it remains low under all conditions of prestress and subsequent measurement load. The permeability increases with increasing level and number of cycles of prestress, shows a smaller rate of increase with increasing strain rate, and generally increases more rapidly with stress in the filling direction than in the warp direction. This behavior is in general qualitative agreement with the trends previously found for a similar fabric, though at a very much lower level of permeability. It seems probable that the two types of behavior found are characteristic of coating weights a little below and a little above the critical value needed to fill all the interstices, and to create a coherent layer of coating material which will withstand repeated stressing.

REFERENCES

1. Alexander, William C., and Lau, Richard A.: State-of-the-Art Study for High-Speed Deceleration and Stabilization Devices, NASA CR-66141, 1966.

2. Mikulas, Martin M., Jr., and Bohon, Herman L.: Development Status of Attached Inflatable Decelerators. J. Spacecraft Rockets, Vol. 6, No. 6, Pp 654-660, June 1969.

3. Bohon, Herman L., and Miserentino, R.: Attached Inflatable Decelerator Performance Evaluation and Mission-Application Study, AAIA Paper No. 70-1163, September 1970.

4. Deaton, Jerry W.: Air Permeability Studies of a Lightweight Coated Fabric Subjected to Uniaxial Tensile Loads With and Without Prior Cycling, NASA TN D-5931.

5. Sebring, Robert E., Freeston, W. D., Jr., Platt, Milton M., Coskren, Robert J.: Mechanical Properties of High Temperature Fibrous Structural Materials, Part III - High-Speed, High Temperature Tensile Tester Technical Report, AFML-TR-67-267, Part III, October 1967.

6. Freeston, W. D., Jr.: Flexible Fibrous Structural Materials, Technical Report, AFML-TR-65-118, April 1965.

7. Davidson, D. A.: The Mechanical Behavior of Fabrics Subjected to Biaxial Stress, ML-TDR-64-239, July 1964.

8. Skelton, J., Freeston, W. D. Jr., and Ford, Harvey K.: The Tensile Behavior of Fibrous Materials at High Rates of Strain and Subambient Temperatures, Applied Polymer Symposia, No. 12, Pp 111-135, 1964.

TABLE 1

CONSTRUCTIONAL DETAILS OF NOMEX FABRICS

	As Received	Calendered	Coated
Ends/in. x Picks/in.	80 x 92	83 x 94	83 x 93
(Ends/cm) x (Picks/cm)	(31.5)x(36.2)	(32.7)x(37.0)	(32.7)x(36.6)
Mass, ozm/yd^2 (Kg/m^2)	2.4(0.08)	2.5(0.09)	2.9(0.10)
Thickness, inch (cm)	5.2×10^{-3} (1.3×10^{-2})	4.2×10^{-3} (1.1×10^{-2})	4.9×10^{-3} (1.2×10^{-2})
Air Permeability at 0.5 inch water, (124N/m^2), ft^3/min/ft^2 (m^3/s/m^2)	8.6(0.4)	3.3(0.2)	1.0×10^{-2} (0.5×10^{-3})

TABLE 2

UNIAXIAL TENSILE BEHAVIOR OF VITON-COATED NOMEX FABRIC AT VARIOUS STRAIN RATES

Strain Rate (%/s)	Warp		Filling	
	Breaking Load, lb/in (kN/m)	Breaking Elongation, (%)	Breaking Load, lb/in (kN/m)	Breaking Elongation, (%)
1	91	19.8	102	28.8
	90	17.7	102	28.5
	93	20.4	103	30.1
	95	21.6	103	29.4
	92	19.2	102	29.1
	92.2 (16.1)	19.7	102.4 (17.9)	29.1
10	103	25.2	115	34.9
	102	26.4	112	34.3
	100	26.4	112	36.1
	98	24.0	114	32.5
	100	26.4	108	31.3
	100.6 (17.6)	25.6	112.2 (19.6)	33.8
100	92	24.7	102	30.0
	96	21.2	100	30.0
	90	22.3	98	28.2
	94	19.4	100	28.2
	92	21.2	100	30.0
	92.8 (16.2)	21.8	100.0 (17.5)	29.3
1,000	100	25.2	76	19.1
	100	20.0	80	20.9
	96	24.3	84	17.4
	104	20.9	76	19.1
	96	19.1	108	24.3
	99.2 (17.4)	21.9	84.8 (14.8)	20.2
10,000	110	17.8	106	28.9
	110	21.1	80	20.0
	110	17.8	100	26.7
	108	18.9	100	25.5
	106	16.7	94	24.4
	108.8 (19.0)	18.5	96.0 (16.8)	25.1

TABLE 3

UNIAXIAL TENSILE BEHAVIOR OF VITON-COATED NOMEX FABRIC AFTER PRESTRESS AT 1% PER SECOND STRAIN RATE

Number of Cycles of Prestress	Cycling Load, Lp, % of Breaking Load	Warp		Filling	
		Breaking Load, lb/in (kN/m)	Elongation, %	Breaking Load, lb/in (kN/m)	Elongation, %
Uncycled Control Average		92.2 (16.1)	19.7	102.4 (17.9)	29.1
1	25	79	11.3	98	21.7
		92	17.5	97	23.4
		88	19.3	97	21.7
		86.3 (15.1)	16.0	97.3 (17.0)	22.3
1	50	91	20.8	100	19.6
		89	17.6	102	20.5
		91	-	96	19.4
		90.3 (15.8)	19.2	99.3 (17.4)	19.8
1	75	96	20.5	93	16.4
		94	19.3	92	17.1
		97	19.3	92	17.1
		95.7 (16.7)	19.7	92.3 (16.1)	16.9
10	25	90	17.3	98	20.4
		87	15.9	96	20.1
		88	20.5	101	21.7
		88.3 (15.4)	17.9	98.3 (17.2)	20.7
10	50	91	20.0	96	18.1
		91	19.7	97	17.3
		93	19.3	94	18.7
		91.7 (16.0)	19.7	95.7 (16.7)	18.0
10	75	83	15.9	89	13.2
		92	17.3	89	14.2
		86	16.9	95	16.1
		87.0 (15.2)	16.7	91.0 (15.9)	14.5

TABLE 4

UNIAXIAL TENSILE BEHAVIOR OF VITON-COATED NOMEX FABRIC AFTER PRESTRESS AT 10% PER SECOND STRAIN RATE

Number of Cycles of Prestress	Cycling Load, Lp, % of Breaking Load	Warp		Filling	
		Breaking Load, lb/in (kN/m)	Elongation, %	Breaking Load, lb/in (kN/m)	Elongation, %
Uncycled Control Average		92.2 (16.1)	19.7	102.4 (17.9)	29.1
1	25	95	21.0	94	19.6
		93	19.9	88	16.9
		91	20.8	82	18.1
		93.0 (16.3)	20.6	88.0 (15.4)	18.2
1	50	91	16.5	92	18.1
		91	17.8	91	16.3
		91	20.2	100	20.5
		91.0 (15.9)	18.2	94.3 (16.5)	18.3
1	75	92	20.5	98	21.0
		93	20.5	95	19.3
		88	16.6	99	19.9
		91.0 (15.9)	19.2	97.3 (17.0)	20.0
10	25	90	19.3	99	22.2
		91	19.3	98	20.5
		89	17.5	97	21.7
		90.0 (15.7)	18.7	98.0 (17.1)	21.5
10	50	97	21.7	90	17.5
		92	21.8	95	15.4
		92	19.9	94	18.3
		93.7 (16.4)	21.1	93.0 (16.3)	17.1
10	75	92	19.9	96	17.3
		92	17.8	91	15.7
		94	19.6	99	18.7
		92.7 (16.2)	19.1	95.3 (16.7)	17.2

TABLE 5

UNIAXIAL TENSILE BEHAVIOR OF VITON-COATED NOMEX FABRIC AFTER PRESTRESS AT 100% PER SECOND STRAIN RATE

Number of Cycles of Prestress	Cycling Load, Lp, % of Breaking Load	Warp		Filling	
		Breaking Load, lb/in (kN/m)	Elongation, %	Breaking Load, lb/in (kN/m)	Elongation, %
Uncycled Control Average		92.2 (16.1)	19.7	102.4 (17.9)	29.1
1	25	-	-	91	23.5
		103	24.7	102	29.4
		99	25.3	92	25.4
		101.0 (17.7)	25.0	95.0 (16.6)	26.1
1	50	-	-	101	31.1
		88	22.3	99	30.1
		101	23.2	102	30.1
		99.5 (17.4)	22.8	100.7 (17.6)	30.4
1	75	102	22.3	102	27.7
		93	18.2	89	22.9
		97	20.0	92	22.0
		97.3 (17.0)	20.2	94.3 (16.5)	24.2
10	25	94	19.9	96	24.3
		96	22.2	98	24.3
		95	22.2	90	21.0
		95.0 (16.6)	21.4	94.7 (16.6)	23.2
10	50	97	21.7	106	25.3
		86	14.2	105	25.0
		98	22.3	107	24.2
		93.7 (16.4)	19.4	106.0 (18.5)	24.8
10	75	96	20.6	98	22.3
		99	22.4	99	20.5
		97	19.9	98	20.5
		97.3 (17.0)	21.0	98.3 (17.2)	21.1

TABLE 6

UNIAXIAL TENSILE BEHAVIOR OF VITON-COATED NOMEX FABRIC AFTER PRESTRESS AT 1,000% PER SECOND STRAIN RATE

Number of Cycles of Prestress	Cycling Load, Lp, % of Breaking Load	Warp		Filling	
		Breaking Load, lb/in (kN/m)	Elongation, %	Breaking Load, lb/in (kN/m)	Elongation, %
Uncycled Control Average		92.2 (16.1)	19.7	102.4 (17.9)	29.1
1	25	93	21.2	85	17.2
		94	23.5	91	18.4
		96	23.7	87	17.5
		94.3 (16.5)	22.8	87.7 (15.3)	17.7
1	50	96	22.9	103	20.0
		93	21.1	104	22.3
		92	21.1	100	21.7
		93.7 (16.4)	21.7	102.3 (17.9)	21.3
1	75	95	22.3	98	21.7
		94	20.0	100	22.0
		93	22.3	105	22.0
		94.0 (16.4)	21.5	101.0 (17.7)	21.9
10	25	94	21.8	99	21.7
		96	21.8	95	18.5
		94	21.8	94	18.1
		94.7 (16.6)	21.8	96.0 (16.8)	19.4
10	50	92	18.1	89	14.0
		91	19.3	89	19.3
		80	13.2	89	18.2
		87.7 (15.3)	16.9	89.0 (15.6)	17.2
10	75	95	21.7	96	19.3
		91	21.1	98	19.3
		88	18.1	102	20.5
		91.3 (16.0)	20.3	98.7 (17.3)	19.7

TABLE 7

UNIAXIAL TENSILE BEHAVIOR OF VITON-COATED NOMEX FABRIC AFTER PRESTRESS AT 10,000% PER SECOND STRAIN RATE

Number of Cycles of Prestress	Cycling Load, Lp, % of Breaking Load	Warp		Filling	
		Breaking Load, lb/in (kN/m)	Elongation, %	Breaking Load, lb/in (kN/m)	Elongation, %
Uncycled Control Average		92.2 (16.1)	19.7	102.4 (17.9)	29.1
1	25	88	17.6	77	14.4
		90	18.1	90	99.6
		92	21.4	82	15.7
		90.0 (15.7)	19.0	83.0 (14.5)	16.6
1	50	94	21.2	98	24.1
		93	19.0	98	20.6
		92	19.6	96	22.9
		93.0 (16.3)	19.9	97.3 (17.0)	22.5
1	75	93	21.2	99	22.9
		92	21.2	94	21.2
		90	20.5	95	20.0
		91.7 (16.0)	21.0	96.0 (16.8)	21.6
10	25	92	19.3	94	20.6
		95	20.5	95	20.6
		92	20.5	97	19.3
		93.0 (16.3)	20.1	95.3 (16.7)	20.2
10	50	90	19.9	94	22.3
		91	19.4	92	23.4
		91	19.3	96	23.5
		90.7 (15.9)	19.5	94.0 (16.4)	23.1
10	75	95	21.8	-	-
		91	19.9	102	22.9
		92	21.2	96	21.7
		92.7 (16.2)	21.0	99.0 (17.3)	22.3

TABLE 8

AIR PERMEABILITY OF VITON-COATED NOMEX FABRIC STRESSED UNIAXIALLY AT A STRAIN RATE OF 1% PER SECOND

Number of Cycles of Prestress	Cycling Load, Lp, % of Breaking Load	Load At Which Permeability Measured, Lm, % of Breaking Load	Air Permeability, $ft^3/min/ft^2$ ($m^3/s/m^2$) Warp	Filling
1	25	10	1.7×10^{-2}	1.2×10^{-2}
			1.8	2.3
			1.9	-
			1.8 (0.9×10^{-3})	1.7 (0.9×10^{-3})
		60	1.9	-
			2.0	2.9
			2.0	2.8
			2.0 (1.0)	2.8 (1.4)
		80	2.3	-
			2.5	3.6
			2.6	3.9
			2.5 (1.2)	3.7 (1.9)
1	50	10	1.2	1.6
			1.2	1.6
			1.2	2.1
			1.2 (0.6)	1.7 (0.9)
		60	1.5	2.7
			1.9	2.9
			1.3	2.5
			1.6 (0.8)	2.7 (1.3)
		80	1.6	3.6
			2.0	3.3
			1.2	3.1
			1.6 (0.8)	3.3 (1.6)
1	75	10	1.2	2.4
			1.3	1.9
			1.3	2.2
			1.3 (0.6)	2.1 (1.1)
		60	1.4	3.6
			1.6	3.2
			1.0	5.2
			1.3 (0.7)	4.0 (2.0)
		80	1.5	4.1
			1.4	3.6
			1.2	4.0
			1.3 (0.7)	3.9 (1.9)

TABLE 8 (Concluded)

AIR PERMEABILITY OF VITON-COATED NOMEX FABRIC STRESSED UNIAXIALLY AT A STRAIN RATE OF 1% PER SECOND

Number of Cycles of Prestress	Cycling Load, Lp, % of Breaking Load	Load At Which Permeability Measured, Lm, % of Breaking Load	Air Permeability, $ft^3/min/ft^2$ ($m^3/s/m^2$) Warp	Filling
10	25	10	1.8×10^{-2}	1.5×10^{-2}
			1.8	-
			1.9	-
			1.8 (0.9×10^{-3})	1.5 (0.7)
		60	2.1	-
			1.9	-
			2.0	2.7
			2.0 (1.0)	2.7 (1.4)
		80	2.3	-
			2.0	-
			2.1	3.5
			2.2 (1.1)	3.5 (1.8)
10	50	10	1.1	2.6
			1.1	2.9
			-	2.3
			1.1 (0.6)	2.6 (1.3)
		60	1.1	4.6
			1.3	4.0
			-	3.8
			1.2 (0.6)	4.1 (2.1)
		80	1.6	5.0
			1.8	4.4
			-	4.4
			1.7 (0.9)	4.6 (2.3)
10	75	10	-	-
			1.7	-
			1.0	5.3
			1.1 (0.5)	5.3 (2.7)
		60	-	-
			2.8	-
			2.2	9.1
			2.5 (1.2)	9.1 (4.5)
		80	-	-
			2.8	-
			2.4	10.2
			2.6 (1.3)	10.2 (5.1)

TABLE 9

AIR PERMEABILITY OF VITON-COATED NOMEX FABRIC STRESSED UNIAXIALLY AT A STRAIN RATE OF 10% PER SECOND

Number of Cycles of Prestress	Cycling Load, Lp, % of Breaking Load	Load At Which Permeability Measured, Lm, % of Breaking Load	Air Permeability, $ft^3/min/ft^2$ ($m^3/s/m^2$) Warp	Filling
1	25	10	2.0×10^{-2}	1.9×10^{-2}
			2.0	2.0
			2.4	2.0
			2.1 (1.1×10^{-3})	2.0 (1.0×10^{-3})
		60	2.3	3.0
			2.0	2.5
			2.9	2.7
			2.4 (1.2)	2.7 (1.4)
		80	2.5	3.4
			2.3	3.4
			2.4	3.0
			2.4 (1.2)	3.2 (1.6)
1	50	10	2.0	1.6
			2.0	1.4
			2.2	1.8
			2.1 (1.1)	1.6 (0.8)
		60	2.2	2.6
			2.3	2.5
			2.3	2.9
			2.3 (1.2)	2.6 (1.3)
		80	2.5	3.1
			2.5	2.7
			2.4	2.8
			2.5 (1.3)	2.8 (1.4)
1	75	10	1.1	1.7
			1.0	3.7
			1.2	1.4
			1.1 (0.5)	2.2 (1.1)
		60	1.5	2.3
			1.0	2.7
			1.8	2.9
			1.4 (0.7)	2.6 (1.3)
		80	1.4	3.7
			0.7	4.0
			1.8	3.0
			1.3 (0.7)	3.5 (1.8)

TABLE 9 (Concluded)

AIR PERMEABILITY OF VITON-COATED NOMEX FABRIC STRESSED UNIAXIALLY AT A STRAIN RATE OF 10% PER SECOND

Number of Cycles of Prestress	Cycling Load, Lp, % of Breaking Load	Load At Which Permeability Measured, Lm, % of Breaking Load	Air Permeability, $ft^3/min/ft^2$ ($m^3/s/m^2$) Warp	Air Permeability, $ft^3/min/ft^2$ ($m^3/s/m^2$) Filling
10	25	10	2.1×10^{-2}	1.6×10^{-2}
			4.5	1.7
			1.4	1.8
			2.6 (1.3×10^{-3})	1.7 (0.8×10^{-3})
		60	2.7	2.3
			5.9	2.3
			2.5	2.6
			3.7 (1.8)	2.4 (1.2)
		80	2.5	3.0
			6.5	3.0
			2.5	3.1
			3.8 (1.9)	3.0 (1.5)
10	50	10	-	-
			2.3	1.9
			2.0	1.3
			2.1 (1.1)	1.6 (0.8)
		60	2.5	3.1
			2.5	2.8
			-	-
			2.5 (1.3)	2.9 (1.5)
		80	-	-
			3.4	3.4
			2.2	4.1
			2.8 (1.4)	3.7 (1.9)
10	75	10	1.9	2.5
			1.8	2.3
			-	-
			1.8 (0.9)	2.4 (1.2)
		60	2.1	3.5
			2.5	4.8
			-	-
			2.3 (1.2)	4.1 (2.1)
		80	2.5	5.5
			2.6	5.6
			-	-
			2.5 (1.3)	5.5 (2.7)

TABLE 10

AIR PERMEABILITY OF VITON-COATED NOMEX FABRIC STRESSED UNIAXIALLY AT A STRAIN RATE OF 100% PER SECOND

Number of Cycles of Prestress	Cycling Load, Lp, % of Breaking Load	Load At Which Permeability Measured, Lm, % of Breaking Load	Air Permeability, $ft^3/min/ft^2$ ($m^3/s/m^2$) Warp	Filling
1	25	10	0.8×10^{-2}	0.5×10^{-2}
			0.9	0.5
			0.7	-
			0.8 (0.4×10^{-3})	0.5 (0.2×10^{-3})
		30	0.9	0.7
			1.1	0.9
			0.9	-
			1.0 (0.5)	0.8 (0.4)
		60	1.2	1.2
			1.3	1.6
			1.2	-
			1.2 (0.6)	1.4 (0.7)
1	50	10	0.8	0.4
			0.5	0.5
			0.9	0.7
			0.7 (0.4)	0.6 (0.3)
		30	0.8	0.8
			0.9	1.0
			1.4	0.8
			1.0 (0.5)	0.8 (0.4)
		60	1.0	1.5
			1.0	1.6
			1.5	1.7
			1.2 (0.6)	1.6 (0.8)
1	75	10	1.0	0.6
			0.8	0.5
			0.8	0.6
			0.9 (0.4)	0.6 (0.3)
		30	1.4	1.2
			0.7	0.8
			0.9	1.1
			1.0 (0.5)	1.0 (0.5)
		60	1.2	1.7
			1.2	1.5
			1.6	1.5
			1.3 (0.7)	1.6 (0.8)

TABLE 10 (Concluded)

AIR PERMEABILITY OF VITON-COATED NOMEX FABRIC STRESSED UNIAXIALLY AT A STRAIN RATE OF 100% PER SECOND

Number of Cycles of Prestress	Cycling Load, Lp, % of Breaking Load	Load At Which Permeability Measured, Lm, % of Breaking Load	Air Permeability, $ft^3/min/ft^2$ ($m^3/s/m^2$) Warp	Filling
10	25	10	0.7×10^{-2}	0.6×10^{-2}
			0.9	0.6
			0.8	0.5
			0.8 (0.4×10^{-3})	0.6 (0.3×10^{-3})
		30	1.0	1.1
			1.0	0.9
			0.8	1.1
			0.9 (0.5)	1.0 (0.5)
		60	1.0	2.0
			1.1	1.7
			1.2	1.8
			1.1 (0.6)	1.8 (0.9)
10	50	10	0.7	0.6
			0.8	0.5
			0.9	0.8
			0.8 (0.4)	0.6 (0.3)
		30	0.8	1.0
			1.1	0.9
			1.2	1.2
			1.0 (0.5)	1.0 (0.5)
		60	1.1	1.9
			1.3	1.6
			1.2	2.1
			1.2 (0.6)	1.8 (0.9)
10	75	10	0.8	0.6
			0.6	0.9
			0.6	0.7
			0.7 (0.3)	0.7 (0.3)
		30	1.0	1.5
			0.9	1.4
			0.8	1.2
			0.9 (0.4)	1.3 (0.7)
		60	1.2	1.8
			1.0	2.1
			1.1	2.0
			1.1 (0.5)	1.9 (1.0)

TABLE 11

AIR PERMEABILITY OF VITON-COATED NOMEX FABRIC STRESSED UNIAXIALLY AT A STRAIN RATE OF 1,000% PER SECOND

Number of Cycles of Prestress	Cycling Load, Lp, % of Breaking Load	Load At Which Permeability Measured, Lm, % of Breaking Load	Air Permeability, $ft^3/min/ft^2$ ($m^3/s/m^2$) Warp	Filling
1	25	10	1.0×10^{-2}	0.3×10^{-2}
			0.7	0.3
			0.6	0.2
			0.7 (0.4×10^{-3})	0.3 (0.1×10^{-3})
		60	1.4	1.8
			1.1	1.6
			1.2	1.5
			1.2 (0.6)	1.6 (0.8)
		80w, 75f	1.3	2.3
			1.3	2.5
			1.8	2.0
			1.4 (0.7)	2.2 (1.1)
1	50	10	0.6	0.4
			0.7	0.3
			1.0	0.4
			0.7 (0.3)	0.4 (0.2)
		60	1.3	1.7
			1.0	1.3
			1.4	1.6
			1.2 (0.6)	1.5 (0.7)
		80w, 75f	1.8	1.9
			1.2	2.0
			1.5	2.0
			1.2 (0.6)	2.0 (1.0)
1	75	10	0.7	0.3
			0.6	0.3
			1.0	0.5
			0.8 (0.4)	0.4 (0.2)
		60	1.0	1.3
			1.0	1.6
			1.4	1.7
			1.1 (0.6)	1.5 (0.7)
		80w, 75f	1.5	2.1
			1.4	1.8
			1.4	1.9
			1.4 (0.7)	1.9 (0.9)

TABLE 11 (Concluded)

AIR PERMEABILITY OF VITON-COATED NOMEX FABRIC STRESSED UNIAXIALLY AT A STRAIN RATE OF 1,000% PER SECOND

Number of Cycles of Prestress	Cycling Load, Lp, % of Breaking Load	Load At Which Permeability Measured, Lm, % of Breaking Load	Air Permeability, $ft^3/min/ft^2$ ($m^3/s/m^2$) Warp	Filling
10	25	10	0.8×10^{-2}	0.4×10^{-2}
			0.4	0.5
			0.7	0.4
			0.6 (0.3×10^{-3})	0.4 (0.2×10^{-3})
		60	1.3	1.4
			1.3	1.9
			1.3	2.0
			1.3 (0.6)	1.7 (0.9)
		65	1.4	1.9
			1.4	2.4
			1.4	2.2
			1.4 (0.7)	2.2 (1.1)
10	50	10	1.0	0.1
			1.0	0.6
			0.9	0.8
			1.0 (0.5)	0.5 (0.2)
		60	1.5	1.6
			1.0	1.9
			1.4	2.3
			1.3 (0.7)	1.9 (0.9)
		65	2.5	2.3
			1.5	2.6
			1.5	2.9
			1.8 (0.9)	2.6 (1.3)
10	75	10	0.7	0.6
			0.6	0.7
			1.0	0.6
			0.8 (0.4)	0.6 (0.3)
		60	1.5	2.2
			1.2	2.3
			1.5	2.1
			1.4 (0.7)	2.2 (1.1)
		65	1.7	2.7
			1.2	2.8
			1.7	2.3
			1.5 (0.8)	2.6 (1.3)

TABLE 12

AIR PERMEABILITY OF VITON-COATED NOMEX FABRIC STRESSED UNIAXIALLY AT A STRAIN RATE OF 10,000% PER SECOND

Number of Cycles of Prestress	Cycling Load, Lp, % of Breaking Load	Load At Which Permeability Measured, Lm, % of Breaking Load	Air Permeability, $ft^3/min/ft^2$ ($m^3/s/m^2$) Warp	Filling
1	25	10	0.8×10^{-2}	0.7×10^{-2}
			0.6	1.1
			0.6	0.7
			0.7 (0.3×10^{-3})	0.8 (0.4×10^{-3})
		30	1.2	0.8
			0.7	1.4
			1.8	0.9
			1.2 (0.6)	1.0 (0.5)
		60	1.1	1.0
			0.9	1.5
			1.8	2.0
			1.3 (0.6)	1.5 (0.7)
1	50	10	0.8	0.6
			0.7	0.8
			0.8	0.9
			0.8 (0.4)	0.7 (0.4)
		30	1.2	0.7
			1.1	0.9
			1.4	1.0
			1.2 (0.6)	0.8 (0.4)
		60	1.5	1.0
			1.1	1.1
			1.7	1.3
			1.4 (0.7)	1.1 (0.6)
1	75	10	0.8	0.8
			0.6	0.7
			0.8	0.7
			0.7 (0.4)	0.7 (0.4)
		30	1.0	1.0
			0.8	1.0
			1.0	0.9
			0.9 (0.5)	1.0 (0.5)
		60	1.3	1.5
			0.9	1.3
			1.1	1.4
			1.1 (0.5)	1.4 (0.7

TABLE 12 (Concluded)

AIR PERMEABILITY OF VITON-COATED NOMEX FABRIC STRESSED UNIAXIALLY AT A STRAIN RATE OF 10,000% PER SECOND

Number of Cycles of Prestress	Cycling Load, Lp, % of Breaking Load	Load At Which Permeability Measured, Lm, % of Breaking Load	Air Permeability, $ft^3/min/ft^2$ ($m^3/s/m^2$) Warp	Air Permeability, $ft^3/min/ft^2$ ($m^3/s/m^2$) Filling
10	25	10	0.8×10^{-2}	0.5×10^{-2}
			0.5	0.4
			0.2	0.5
			0.7 (0.3×10^{-3})	0.5 (0.2×10^{-3})
		30	1.0	1.0
			1.2	1.1
			0.4	1.1
			0.8 (0.4)	1.1 (0.6)
		60	1.8	1.7
			1.8	2.3
			1.4	2.2
			1.0 (0.5)	2.1 (1.0)
10	50	10	0.4	0.6
			0.6	0.5
			0.6	0.7
			0.5 (0.3)	0.6 (0.3)
		30	0.7	1.4
			1.1	1.0
			1.2	1.2
			1.0 (0.5)	1.2 (0.6)
		60	1.7	2.5
			2.5	1.8
			2.1	2.1
			2.1 (1.0)	2.1 (1.1)
10	75	10	0.8	0.7
			0.6	1.0
			0.5	0.8
			0.6 (0.3)	0.8 (0.4)
		30	1.3	1.6
			1.2	2.1
			1.1	1.7
			1.2 (0.6)	1.8 (0.9)
		60	2.1	2.7
			1.9	3.4
			1.8	2.6
			1.9 (1.0)	2.8 (1.4)

TABLE 13

AIR PERMEABILITY OF VITON-COATED NOMEX FABRIC STRESSED BIAXIALLY

Number of Cycles of Prestress	Cycling Load, Lp, % of Breaking Load	Load At Which Permeability Measured, Lm, % of Breaking Load	Air Permeability, $ft^3/min/ft^2$ ($m^3/s/m^2$) (Warp Load/Filling Load) 1:1	2:1	1:2
1	25	10	2.5×10^{-2} 1.8 1.6 1.9 (0.9×10^{-3})	1.6×10^{-2} 1.4 1.4 1.5 (0.7×10^{-3})	1.2×10^{-2} 1.5 1.5 1.4 (0.7×10^{-3})
		30	3.0 2.9 2.7 2.8 (1.4)	2.3 1.5 1.6 1.8 (0.9)	1.9 2.0 1.9 1.9 (1.0)
		65	4.1 3.6 3.8 3.8 (1.4)	2.5 2.1 2.2 2.2 (1.1)	2.9 2.9 2.9 2.9 (1.5)
1	50	10	1.8 1.6 2.0 1.8 (0.9)	1.8 2.0 1.8 1.9 (0.9)	1.1 1.8 1.7 1.5 (0.8)
		30	2.9 2.9 3.1 3.0 (1.0)	1.8 2.4 1.9 2.0 (1.0)	2.0 2.1 2.9 2.3 (1.1)
		65	3.7 3.8 4.4 3.9 (2.0)	2.5 2.5 2.7 2.6 (1.3)	3.0 2.7 3.0 2.9 (1.5)

TABLE 13 (Cont.)

AIR PERMEABILITY OF VITON-COATED NOMEX FABRIC STRESSED BIAXIALLY

Number of Cycles of Prestress	Cycling Load, Lp, % of Breaking Load	Load At Which Permeability Measured, Lm, % of Breaking Load	Air Permeability, $ft^3/min/ft^2$ ($m^3/s/m^2$) (Warp Load/Filling Load) 1:1	2:1	1:2
1	65	10	3.0×10^{-2} 3.1 2.8 2.9 (1.5×10^{-3})	1.3×10^{-2} 1.5 1.4 1.4 (0.7×10^{-3})	1.7×10^{-2} 1.4 1.7 1.6 (0.8×10^{-3})
		30	4.2 3.7 4.5 4.1 (2.1)	2.0 2.0 2.1 2.0 (1.0)	2.4 1.8 1.7 1.9 (0.9)
		65	5.2 4.5 4.6 4.7 (2.3)	2.8 3.1 2.8 2.9 (1.5)	2.6 2.8 2.5 2.6 (1.3)
10	25	10	1.8 2.3 1.4 1.8	1.6 1.3 1.7 1.5	1.6 1.6 1.5 1.6
		30	1.8 2.5 1.8 2.0 (1.0)	2.3 1.4 1.9 1.8 (0.9)	2.2 1.6 1.8 1.8 (0.9)
		65	2.9 4.1 2.5 3.1 (1.5)	2.5 2.2 2.5 2.4 (1.2)	2.5 2.3 2.5 2.4 (1.2)

TABLE 13 (Concluded)

AIR PERMEABILITY OF VITON-COATED NOMEX FABRIC STRESSED BIAXIALLY

Number of Cycles of Prestress	Cycling Load, Lp, % of Breaking Load	Load At Which Permeability Measured, Lm, % of Breaking Load	Air Permeability, $ft^3/min/ft^2$ ($m^3/s/m^2$) (Warp Load/Filling Load) 1:1	2:1	1:2
10	50	10	2.5×10^{-2}	1.3×10^{-2}	1.7×10^{-2}
			2.3	1.2	1.6
			1.8	1.3	1.7
			2.2 (1.1×10^{-3})	1.3 (0.7×10^{-3})	1.7 (0.8×10^{-3})
		30	3.4	1.2	2.5
			2.7	1.8	2.2
			2.3	2.0	2.2
			2.8 (1.4)	1.6 (0.8)	2.3 (1.1)
		65	5.2	2.1	3.1
			4.0	2.7	2.8
			3.4	2.5	2.6
			4.2 (2.2)	2.4 (1.2)	2.8 (1.4)
10	65	10	2.0	1.4	1.6
			2.9	1.0	1.5
			3.0	1.6	1.4
			2.6 (1.3)	1.3 (0.7)	1.5 (0.8)
		30	3.5	1.5	2.3
			3.1	1.2	2.2
			3.9	2.1	2.1
			2.5 (1.7)	1.6 (0.8)	2.2 (1.1)
		65	3.2	2.2	2.4
			4.3	2.3	2.9
			5.8	3.0	2.2
			4.4 (2.2)	2.5 (1.2)	2.6 (1.3)

TABLE 14

AIR PERMEABILITY OF VITON-COATED NOMEX FABRIC - UNSTRESSED CONTROL

Load At Which Permeability Measured, Lm, % of Breaking Load	Air Permeability, $ft^3/min/ft^2$ ($m^3/s/m^2$)	
	Warp	Filling
0*	1.0, range 0.6 - 1.6×10^{-2} (0.5, range $0.3 - 0.8 \times 10^{-3}$)	
10	1.0×10^{-2}	0.6×10^{-2}
	1.0	0.7
	1.0	0.7
	1.0	0.8
	1.0	0.7
	1.0 (0.5×10^{-3})	0.7 (0.3×10^{-3})
60	1.1	1.8
	1.4	2.1
	1.4	2.2
	1.5	2.0
	1.6	2.1
	1.4 (0.7)	2.0 (1.0)
80	1.3	2.0
	1.2	2.4
	1.2	2.5
	1.8	2.5
	1.4	2.3
	1.4 (0.7)	2.3 (1.2)

* Large number of measurements made at zero load.

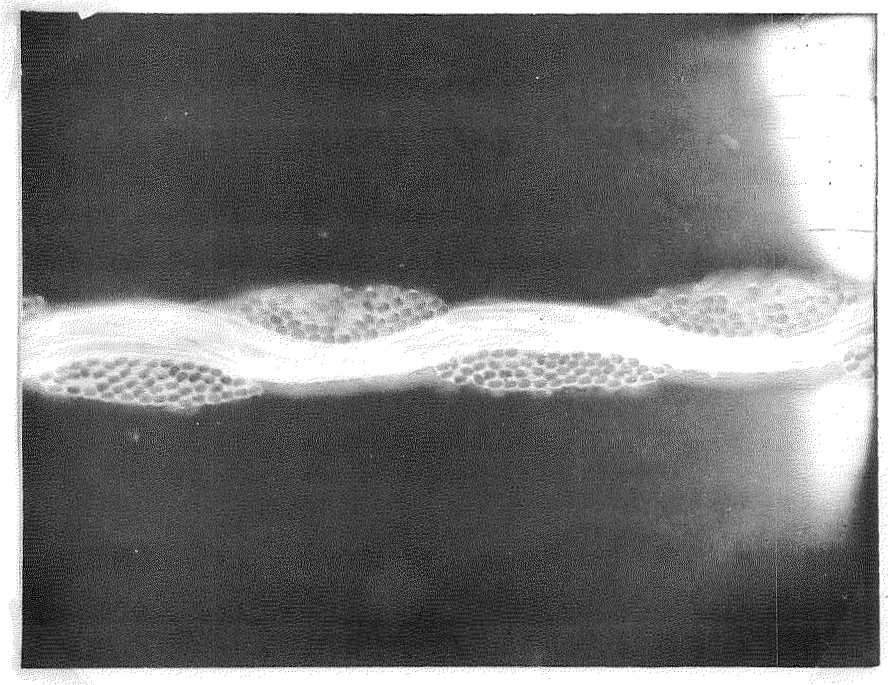

Warp

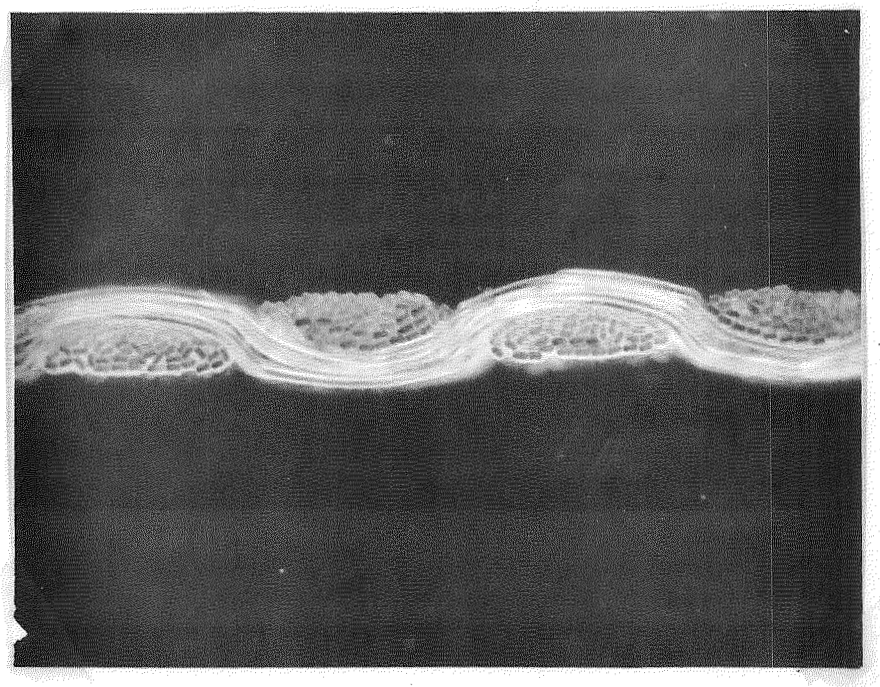

Filling

Figure 1. Sections along Yarns in Viton-Coated Nomex Fabric

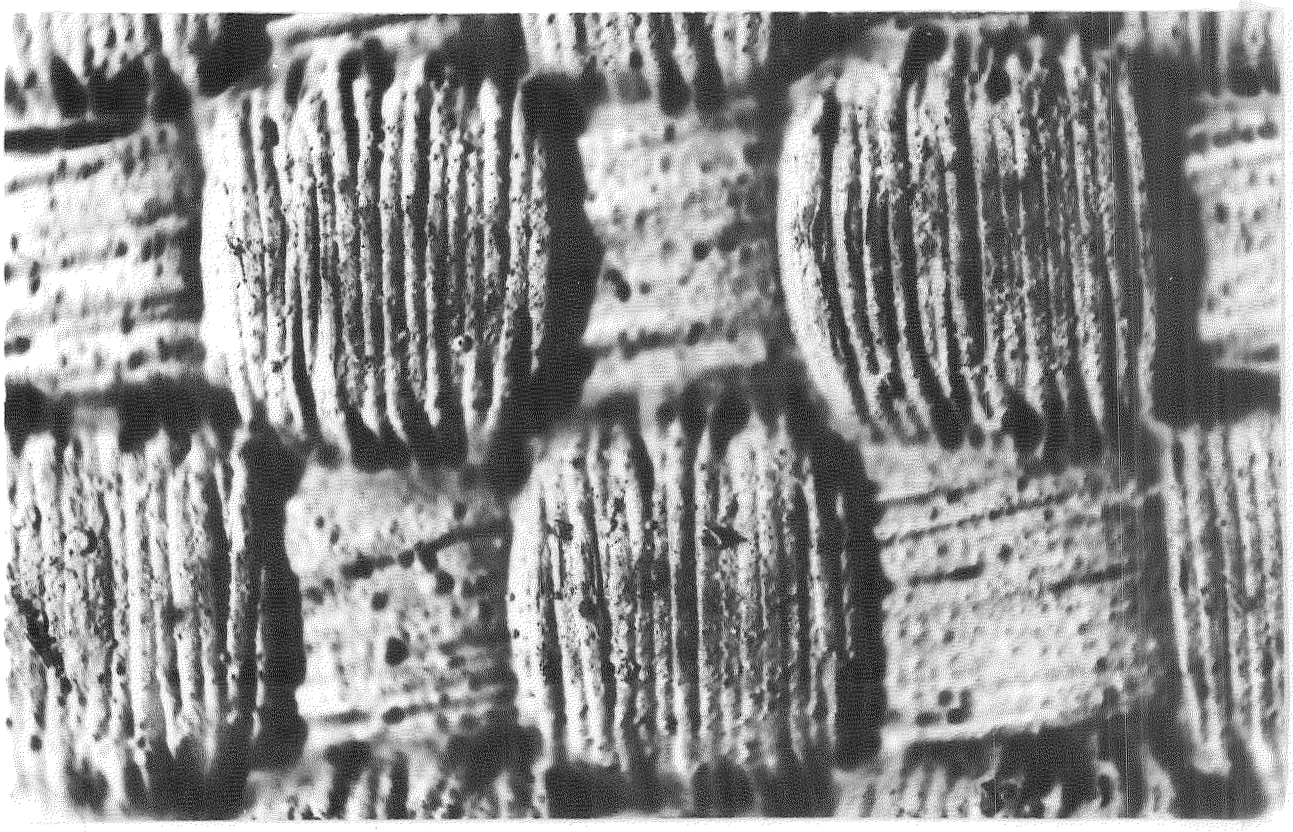

Coated Side

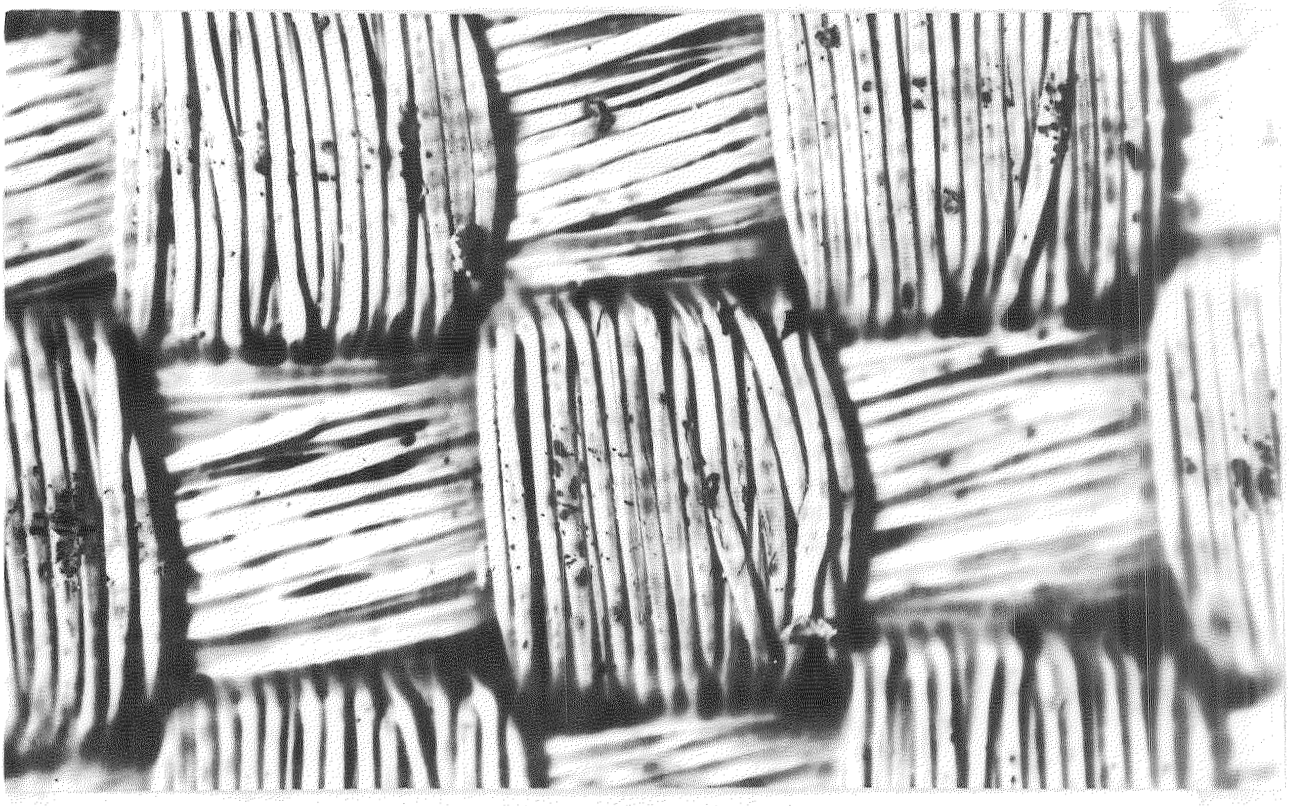

Uncoated Side

Figure 2. Surface Features of Viton-Coated Nomex Fabric

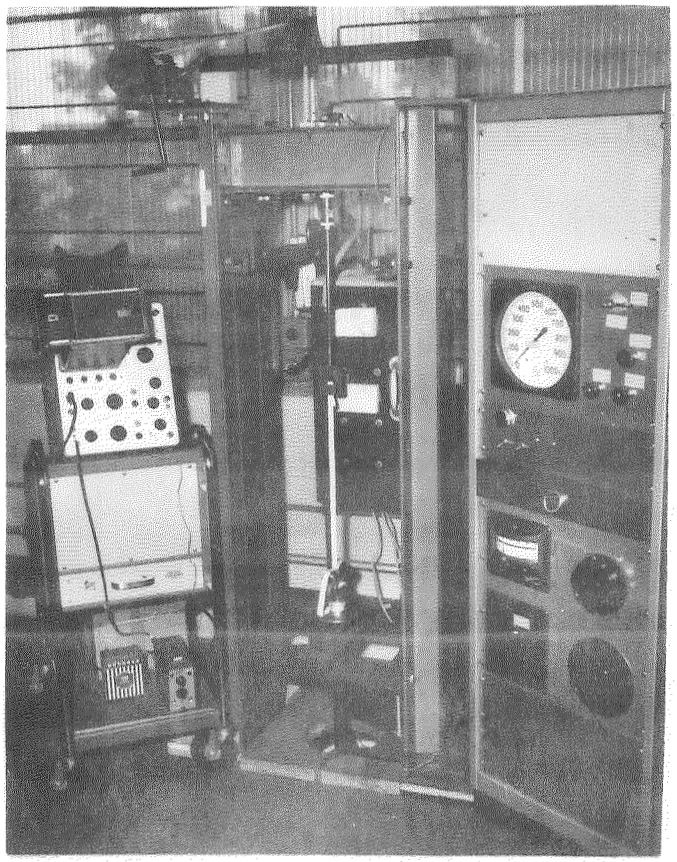

Figure 3. Overall View of FRL® Piston Tester

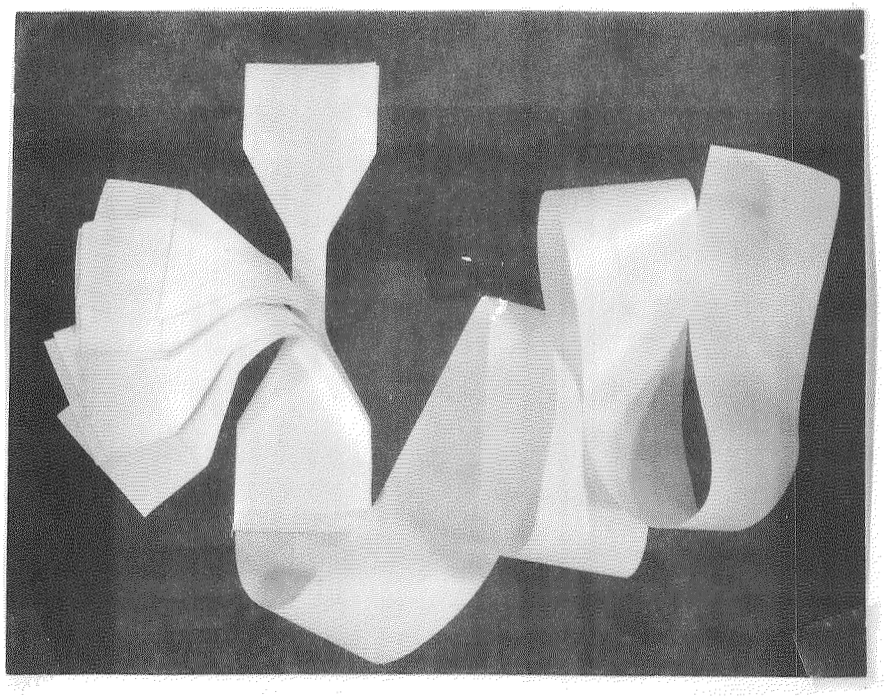

Figure 4. Test Specimen for Multiple Load Cycling at High Strain Rates

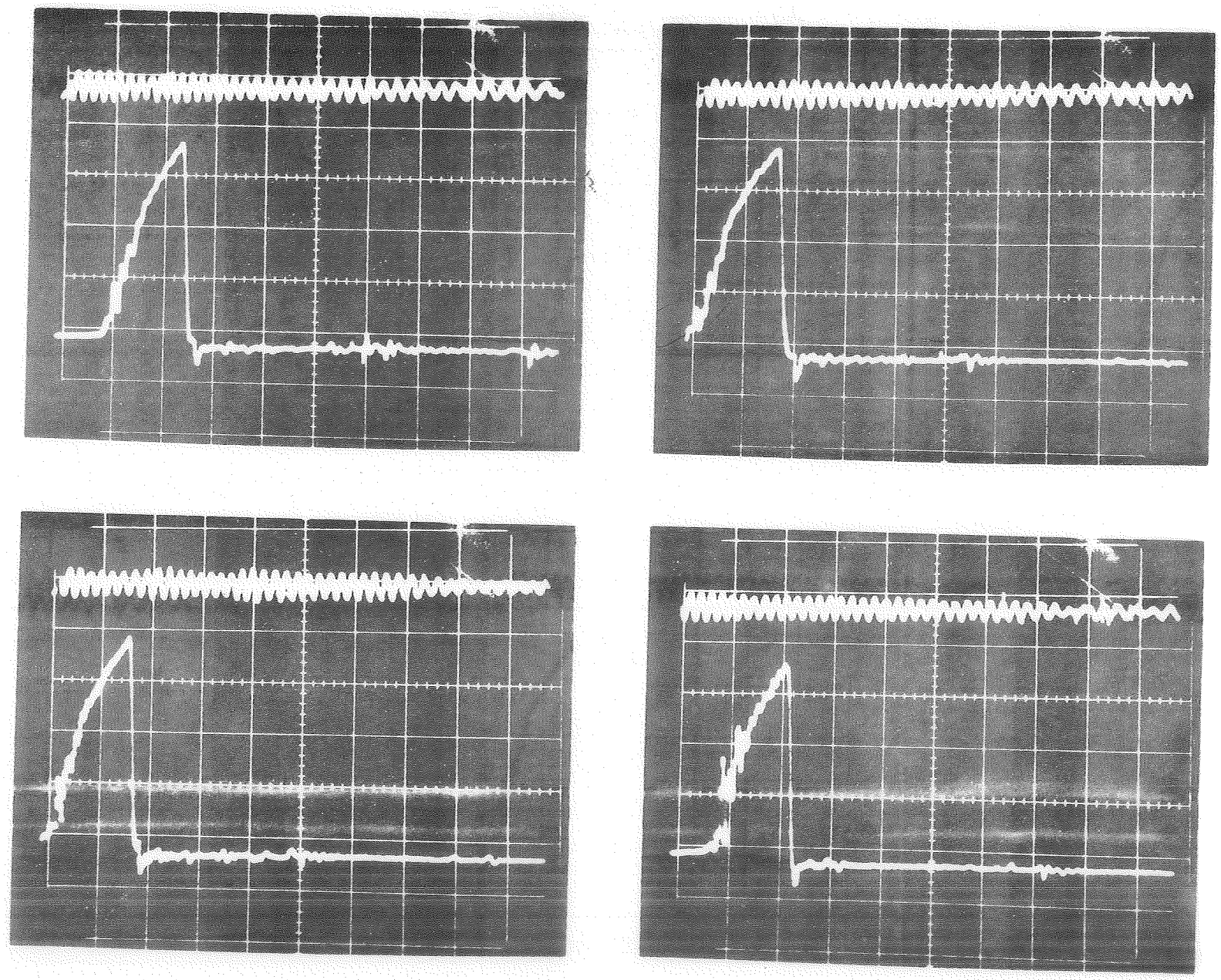

Figure 5. Typical Oscilloscope Traces for Load Cycling to 75% of Breaking Load at 1,000% Per Second

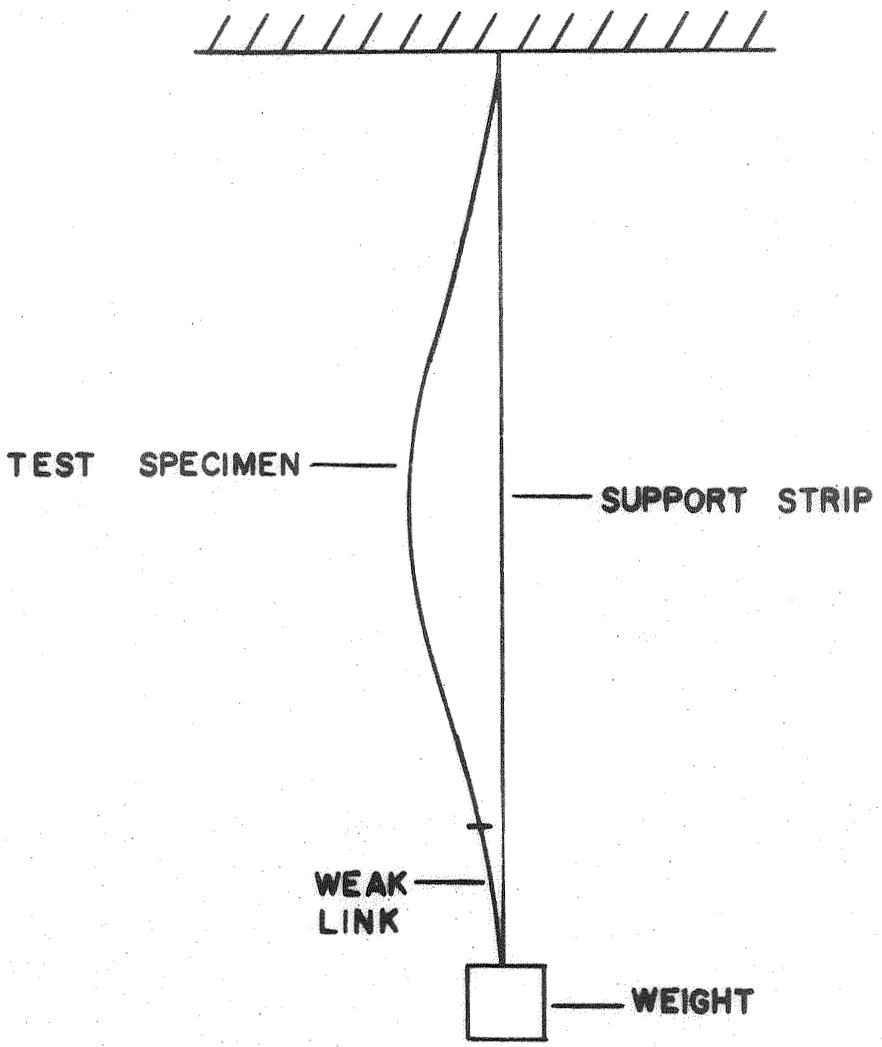

Figure 6. Experimental Arrangement for Drop-Weight Test

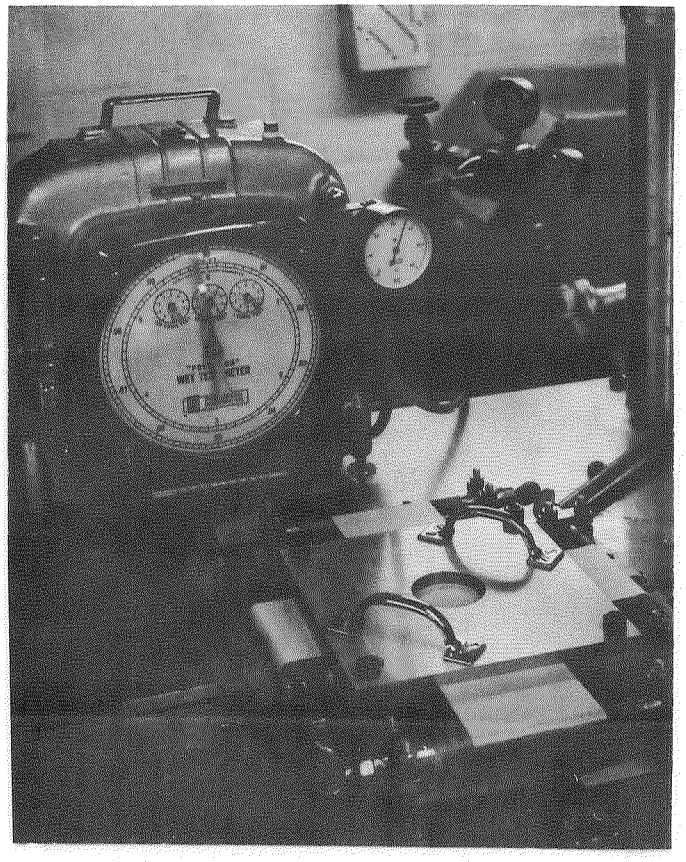

Figure 7. Air Permeability Apparatus

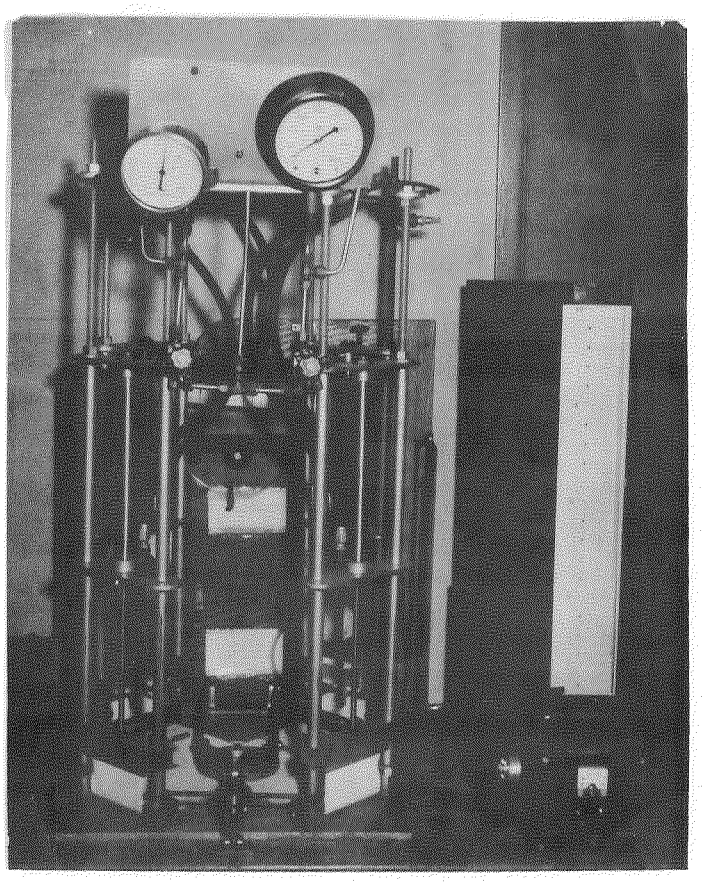

Figure 8. Biaxial Tensioning Device for Permeability Measurements

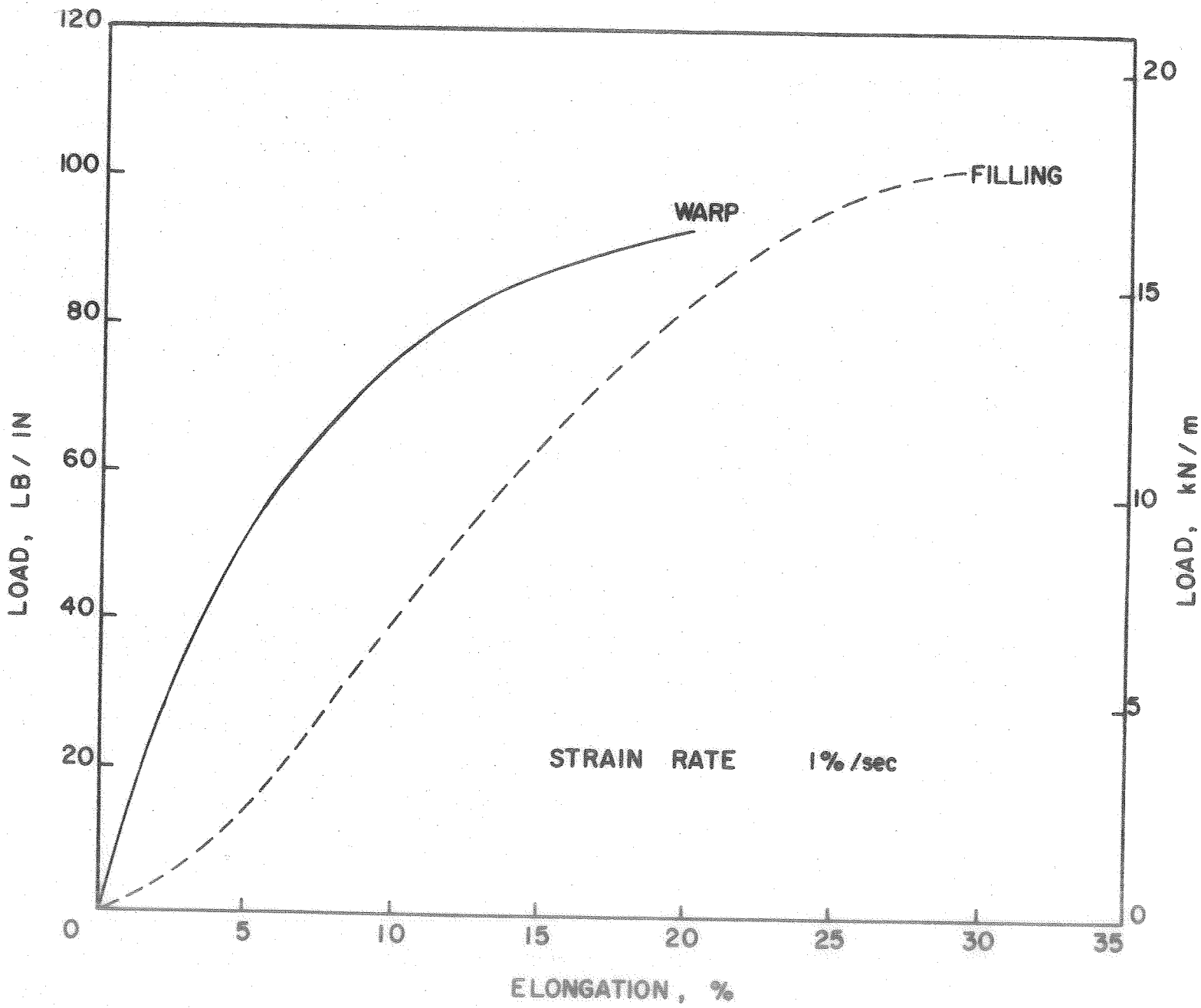

Figure 9. Uniaxial Load-Elongation Curves for Viton-Coated Nomex Fabric - Strain Rate 1% Per Second

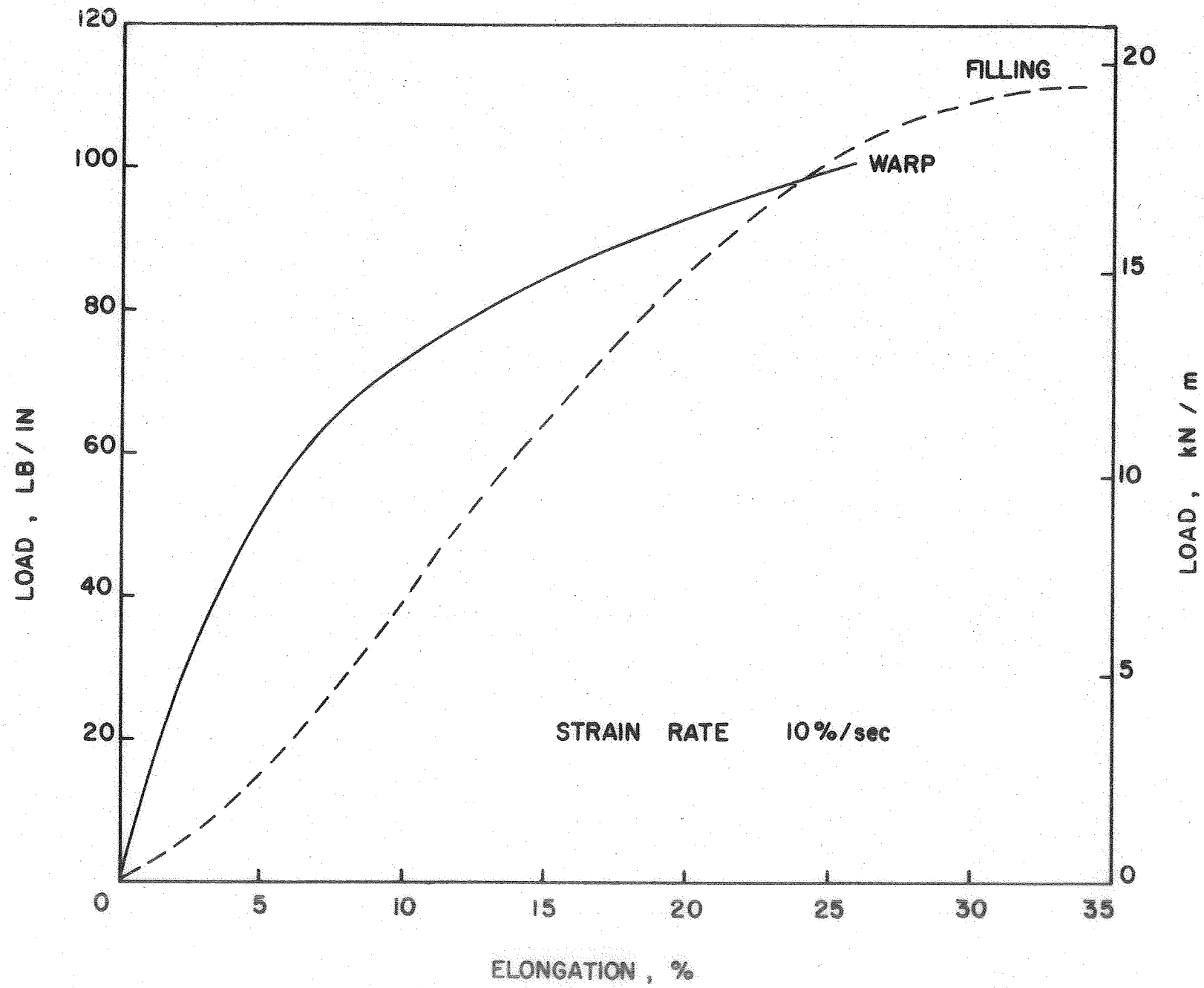

Figure 10. Uniaxial Load-Elongation Curves for Viton-Coated Nomex Fabric - Strain Rate 10% Per Second

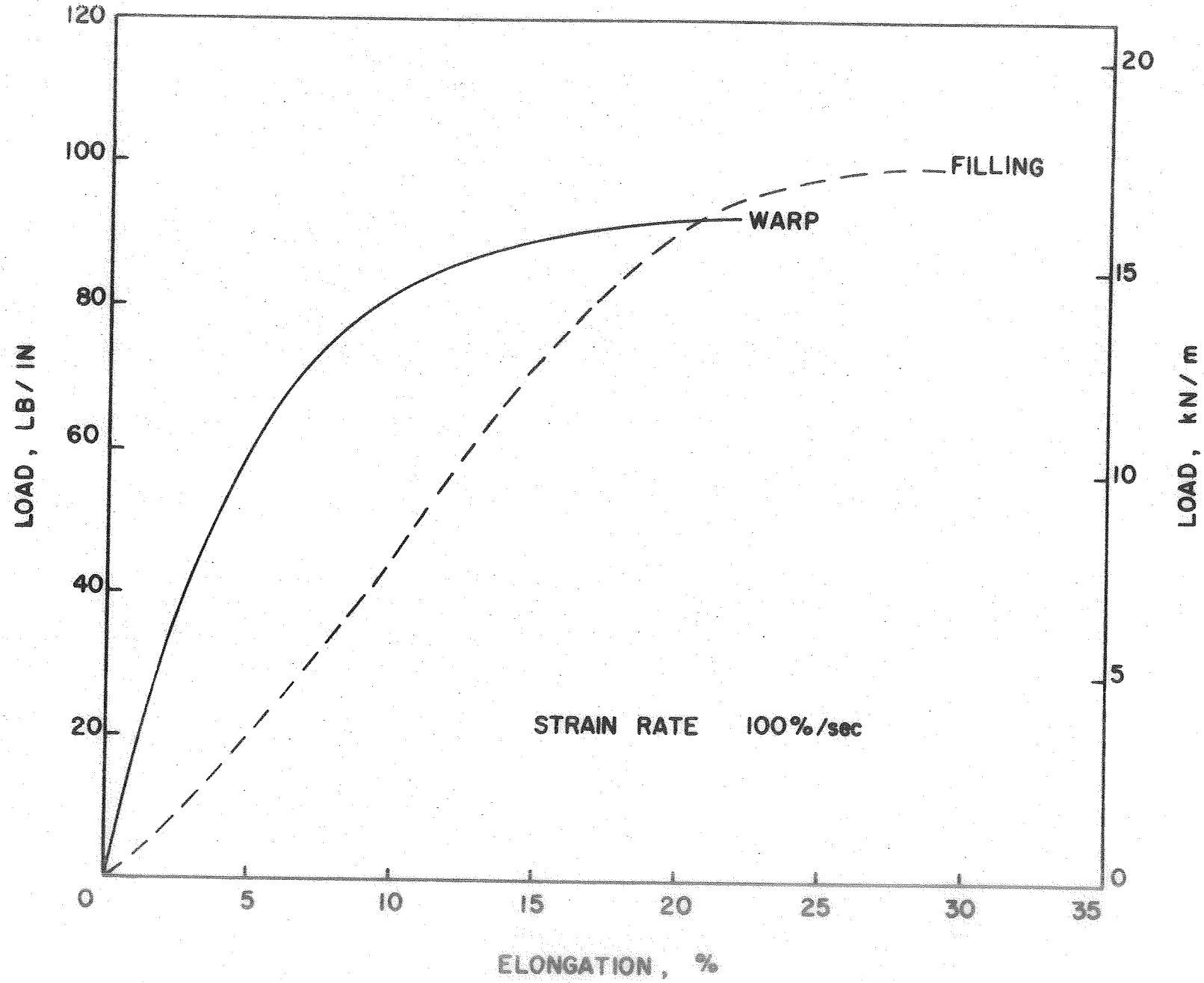

Figure 11. Uniaxial Load-Elongation Curves for Viton-Coated Nomex Fabric - Strain Rate 100% Per Second

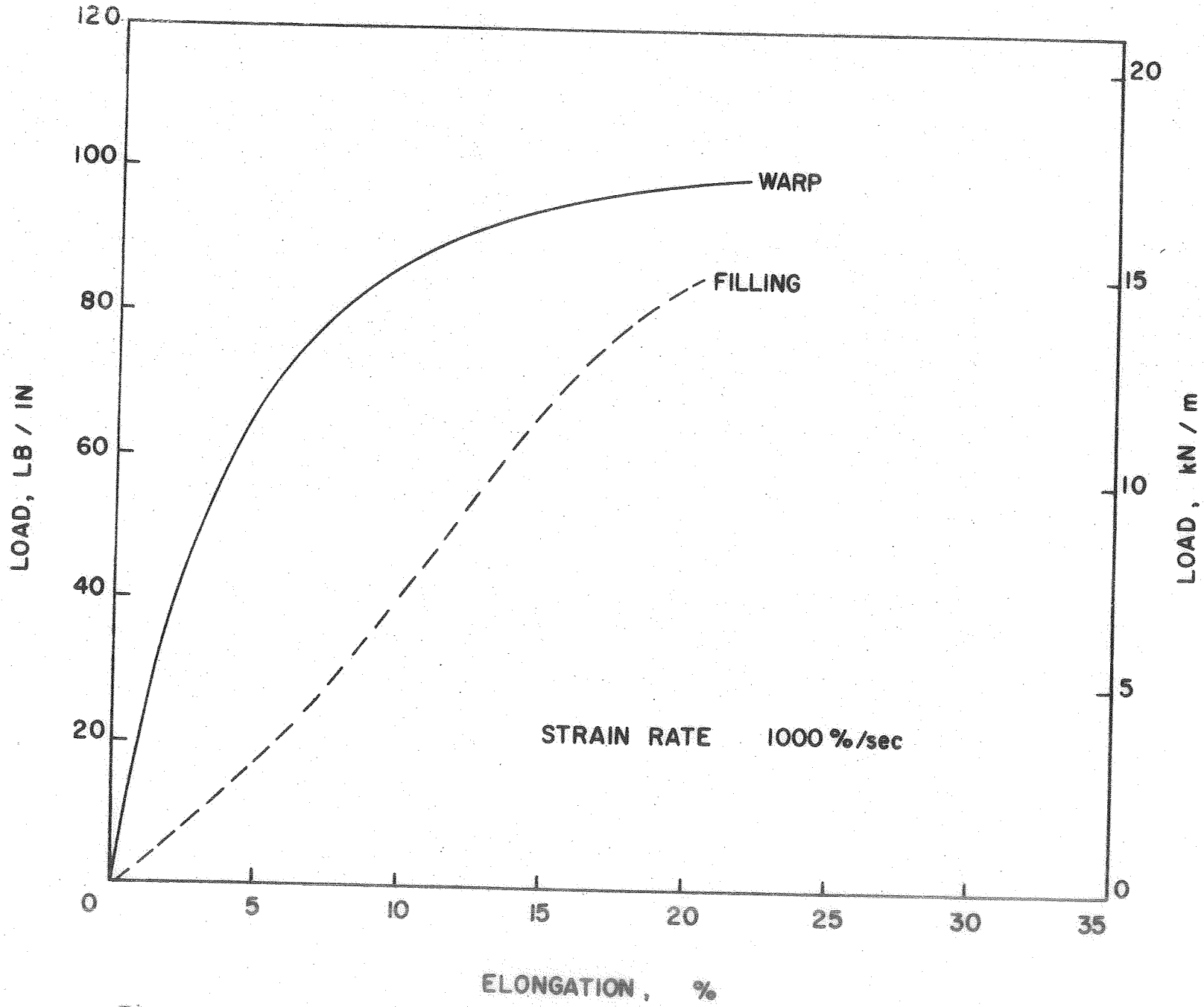

Figure 12. Uniaxial Load-Elongation Curves for Viton-Coated Nomex Fabric - Strain Rate 1,000% Per Second

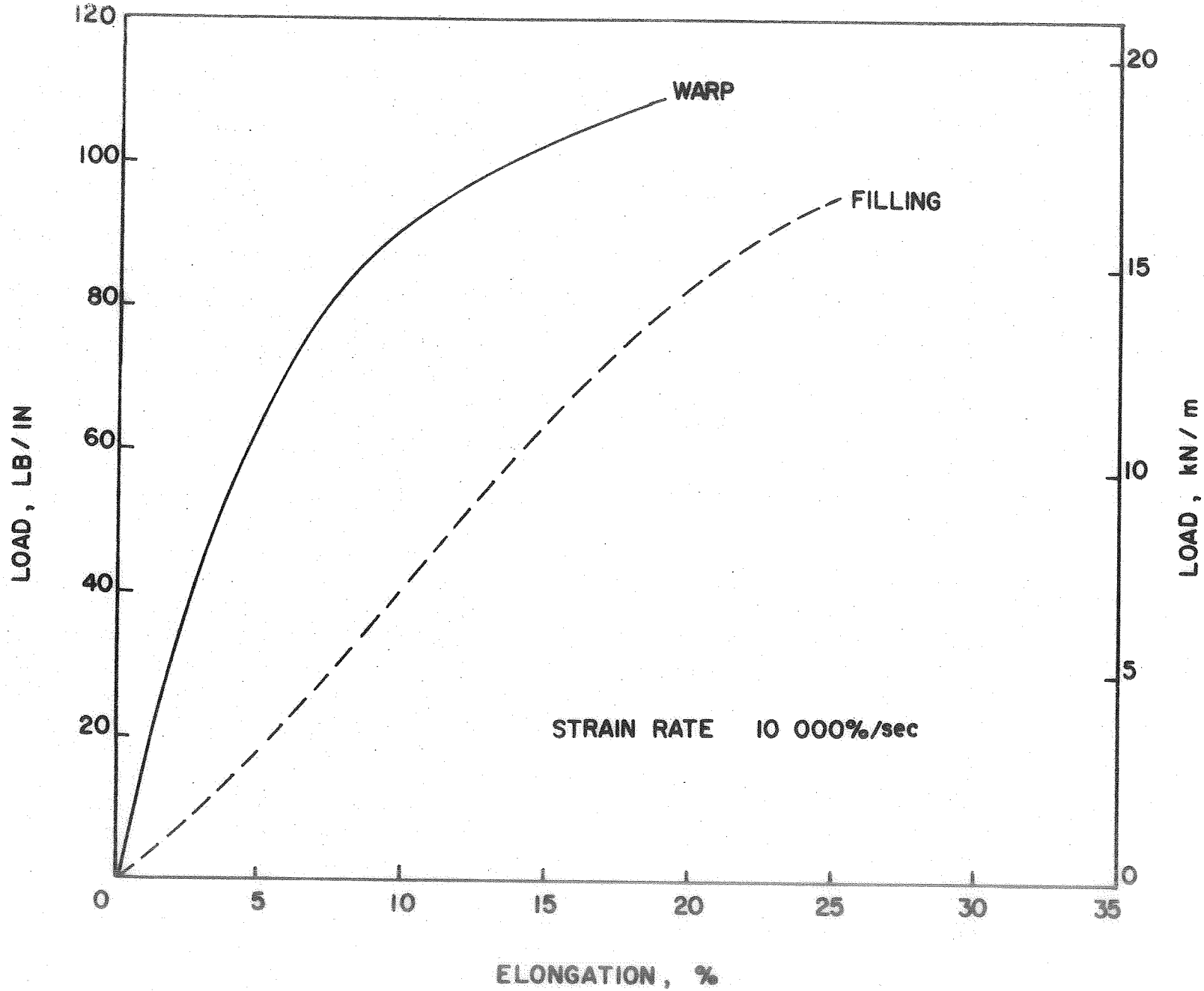

Figure 13. Uniaxial Load-Elongation Curves for Viton-Coated Nomex Fabric - Strain Rate 10,000% Per Second

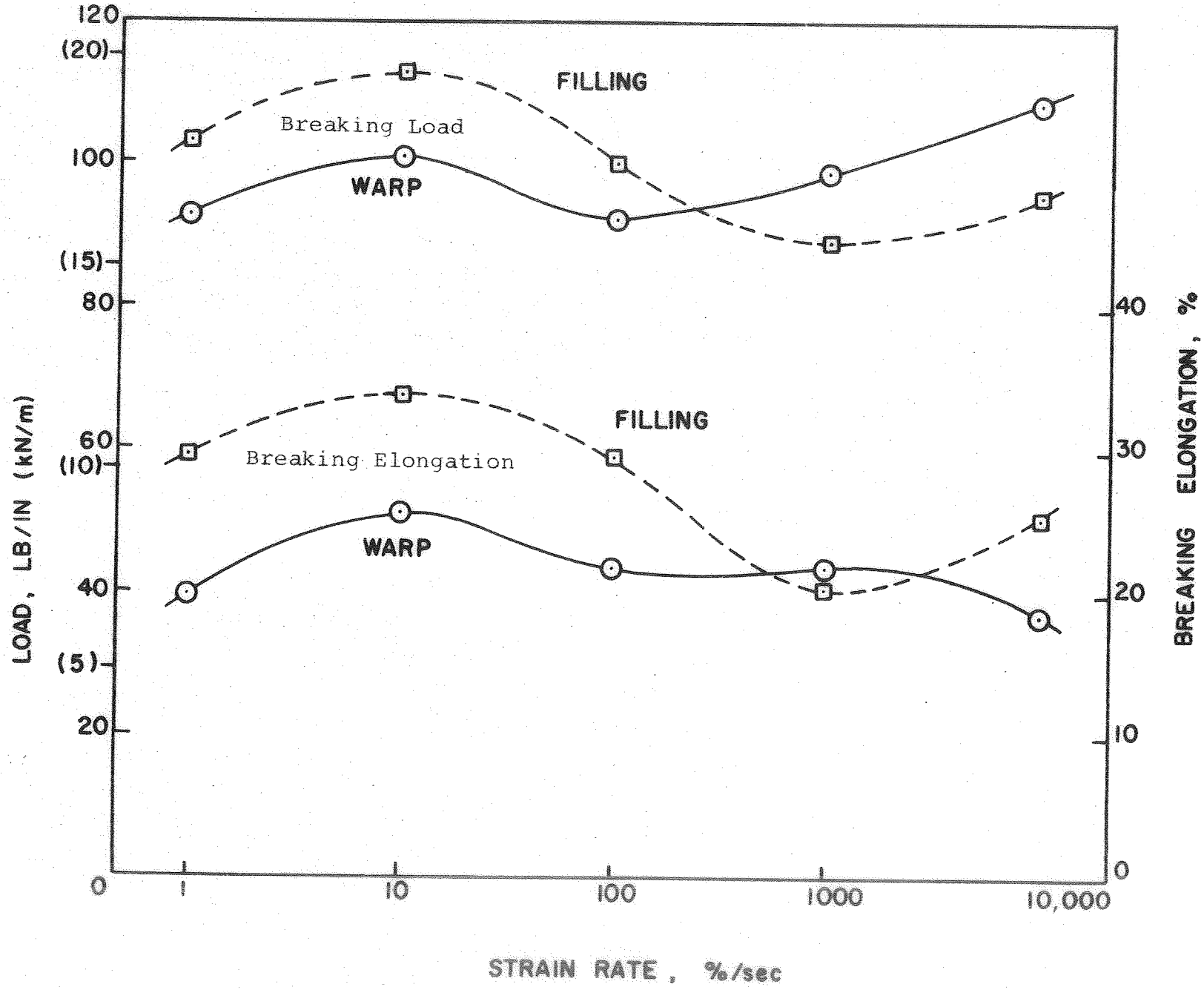

Figure 14. Variation of Breaking Load and Breaking Elongation with Strain Rate for Viton-Coated Nomex Fabric

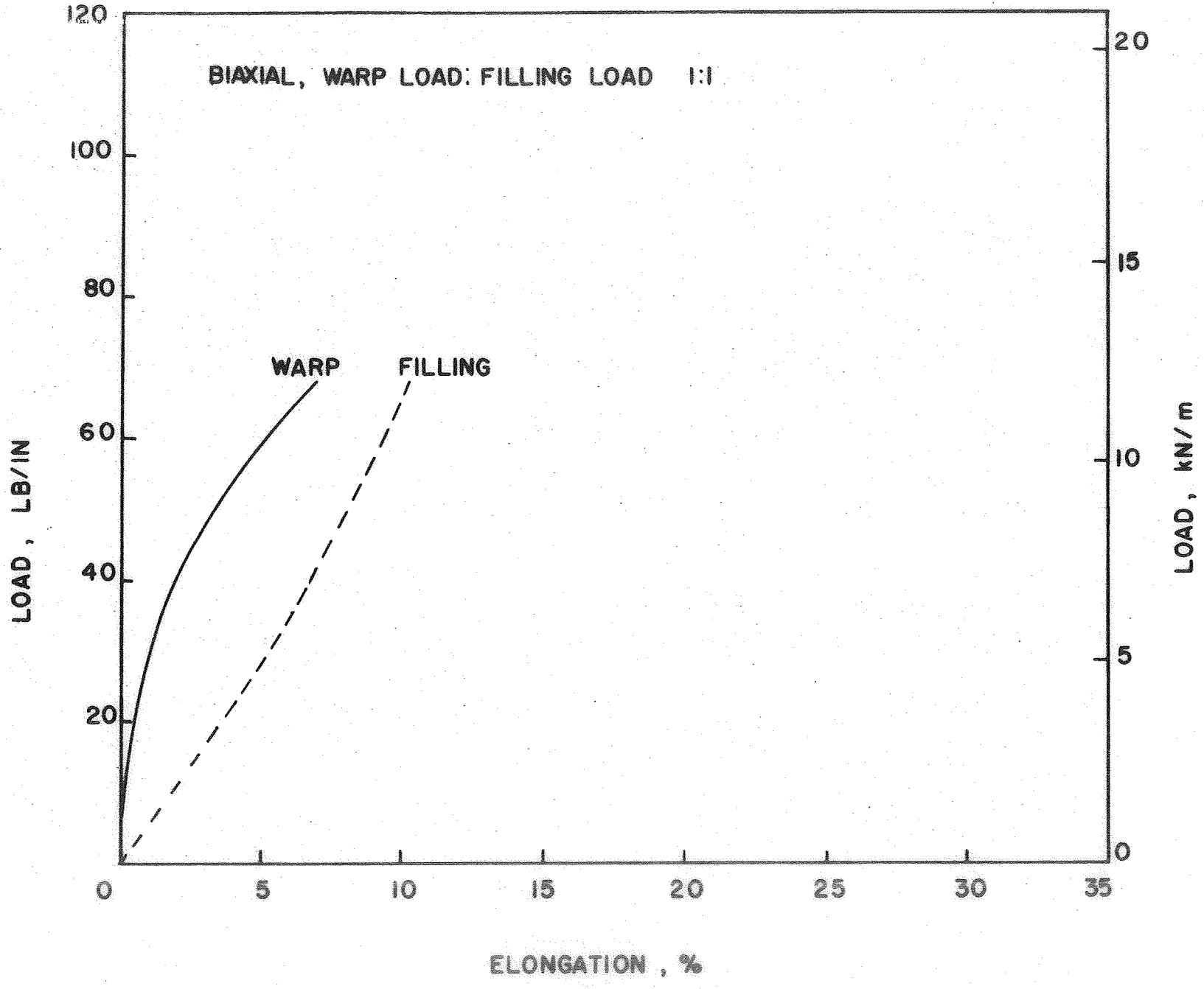

Figure 15. Biaxial Load-Elongation Curves for Viton-Coated Nomex Fabric - Warp Load/Filling Load 1:1

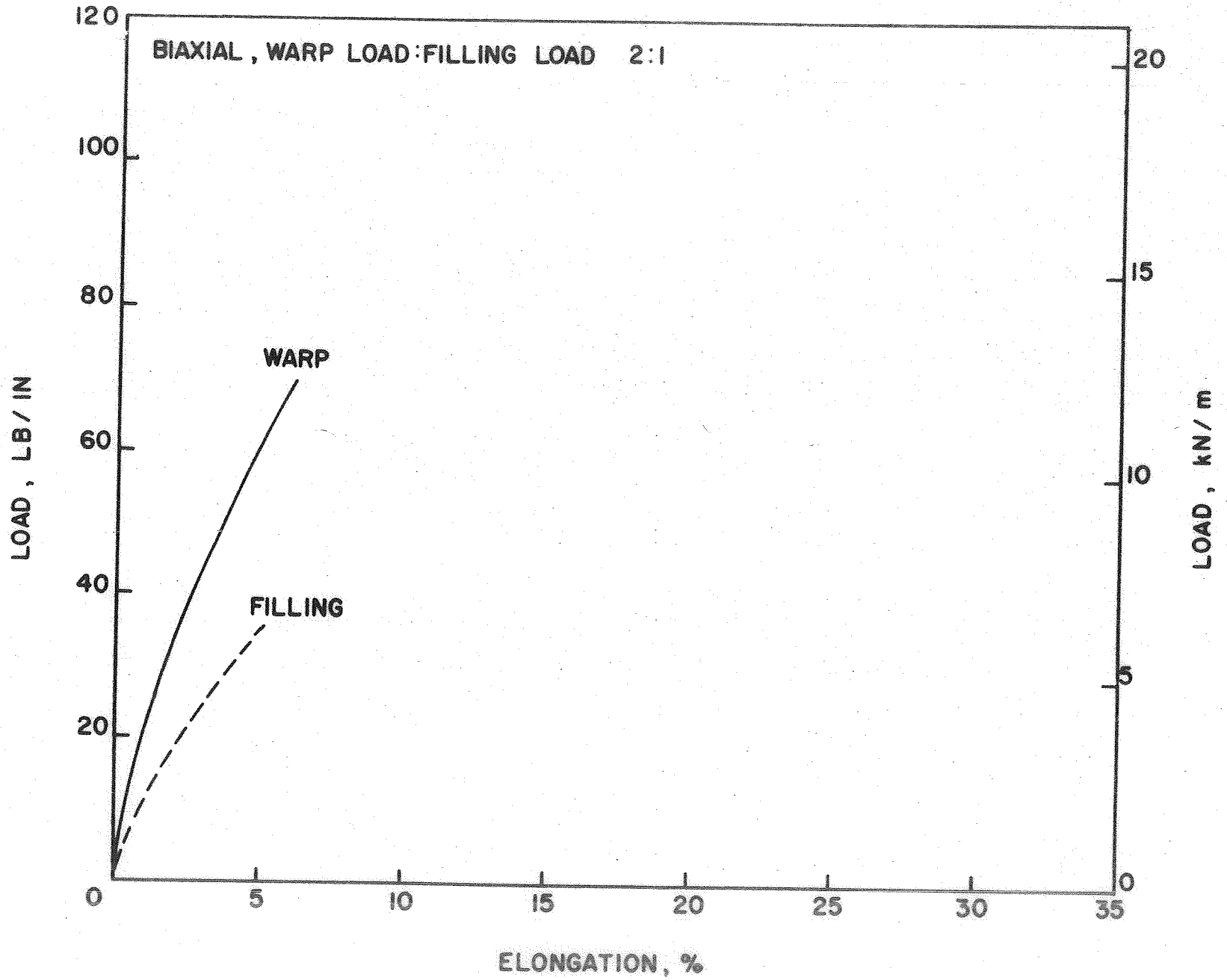

Figure 16. Biaxial Load-Elongation Curves for Viton-Coated Nomex Fabric - Warp Load/Filling Load 2:1

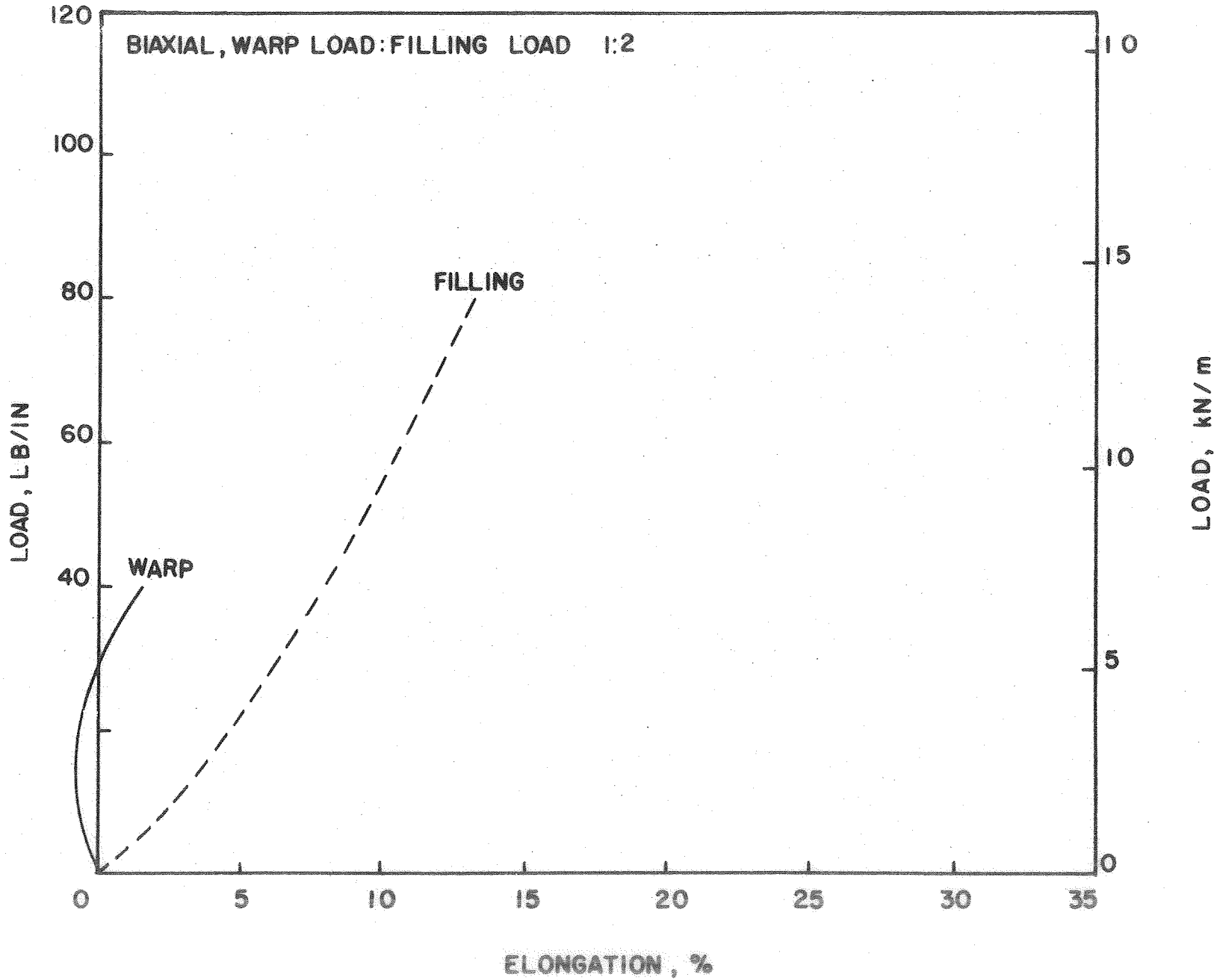

Figure 17. Biaxial Load-Elongation Curves for Viton-Coated Nomex Fabric - Warp Load/Filling Load 1:2

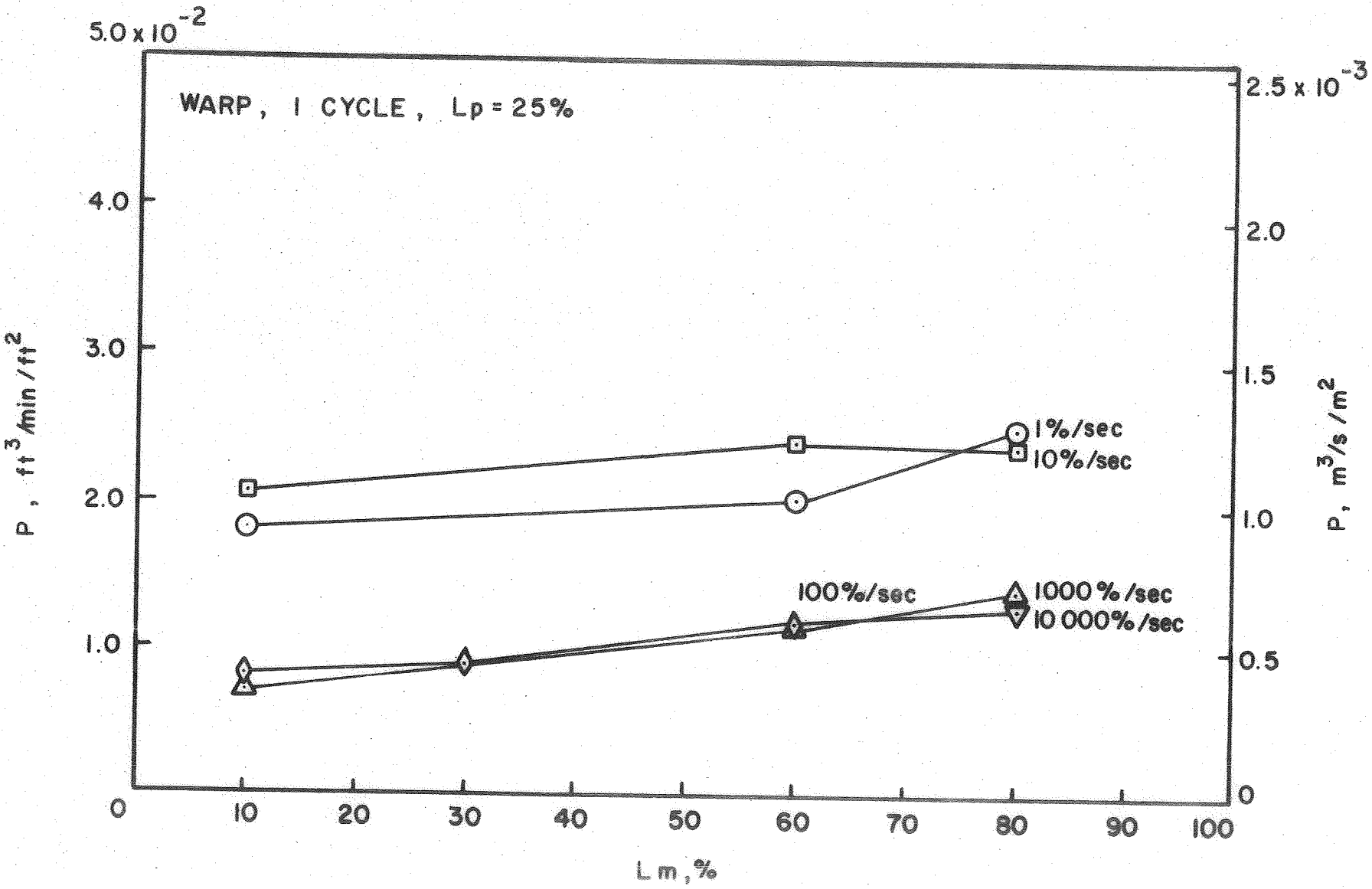

Figure 18. Variation of Air Permeability, P, with Load, Lm, for Fabric Prestressed Uniaxially at Various Strain Rates. Warp Direction, 1 Cycle of Prestress to 25% of Breaking Load

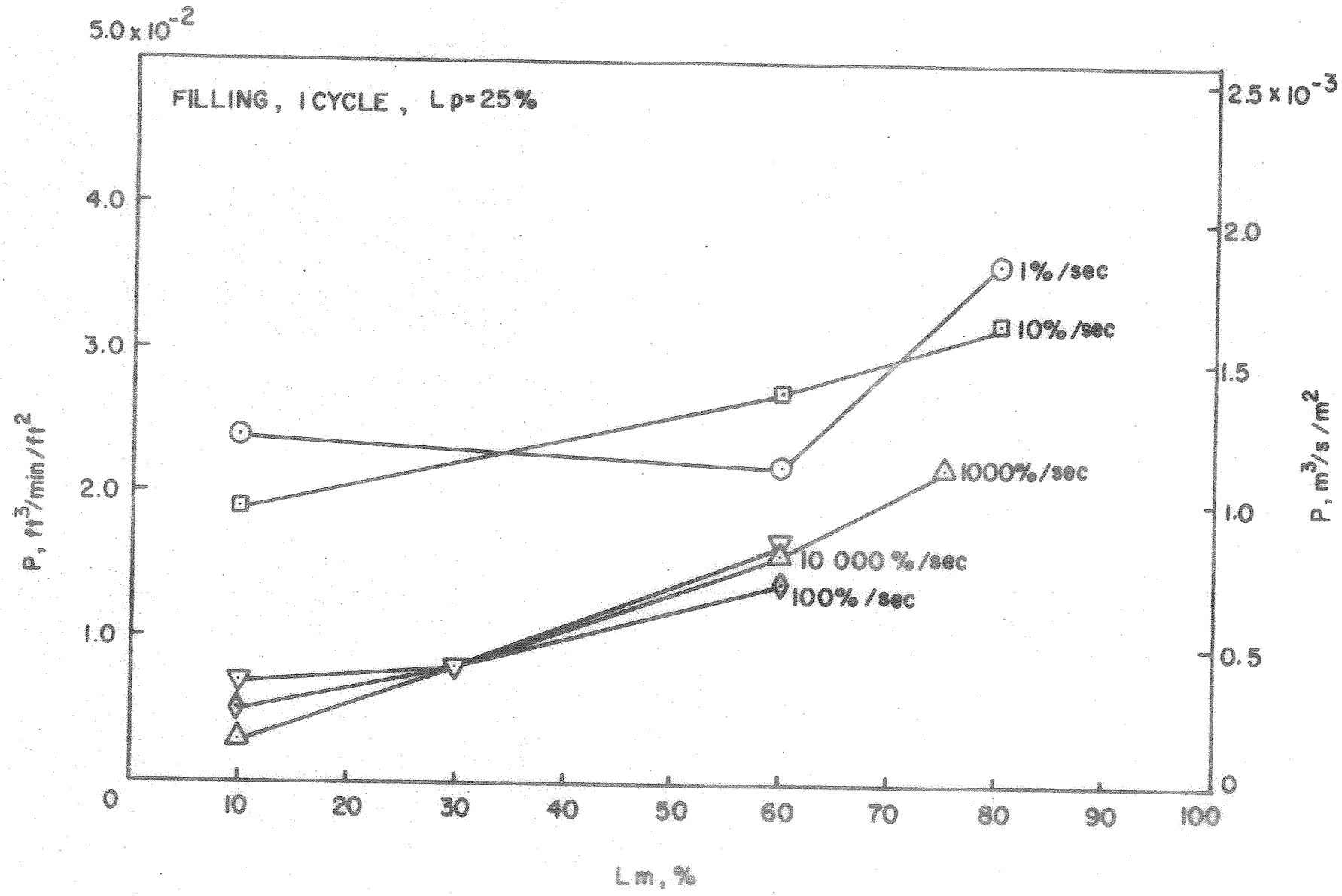

Figure 19. Variation of Air Permeability, P, with Load, Lm, for Fabric Prestressed Uniaxially at Various Strain Rates. Filling Direction, 1 Cycle of Prestress to 25% of Breaking Load

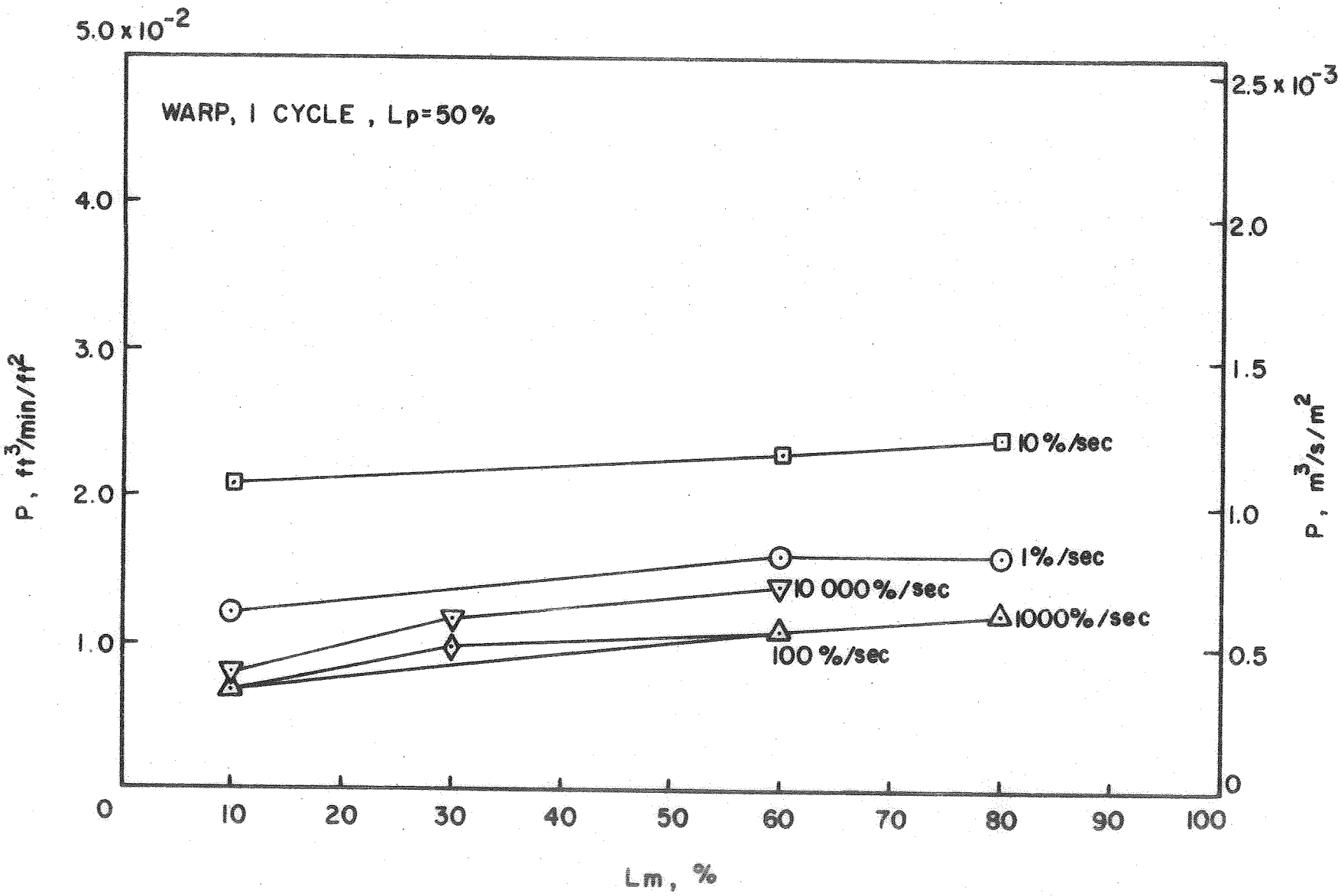

Figure 20. Variation of Air Permeability, P, with Load, Lm, for Fabric Prestressed Uniaxially at Various Strain Rates. Warp Direction, 1 Cycle of Prestress to 50% of Breaking Load

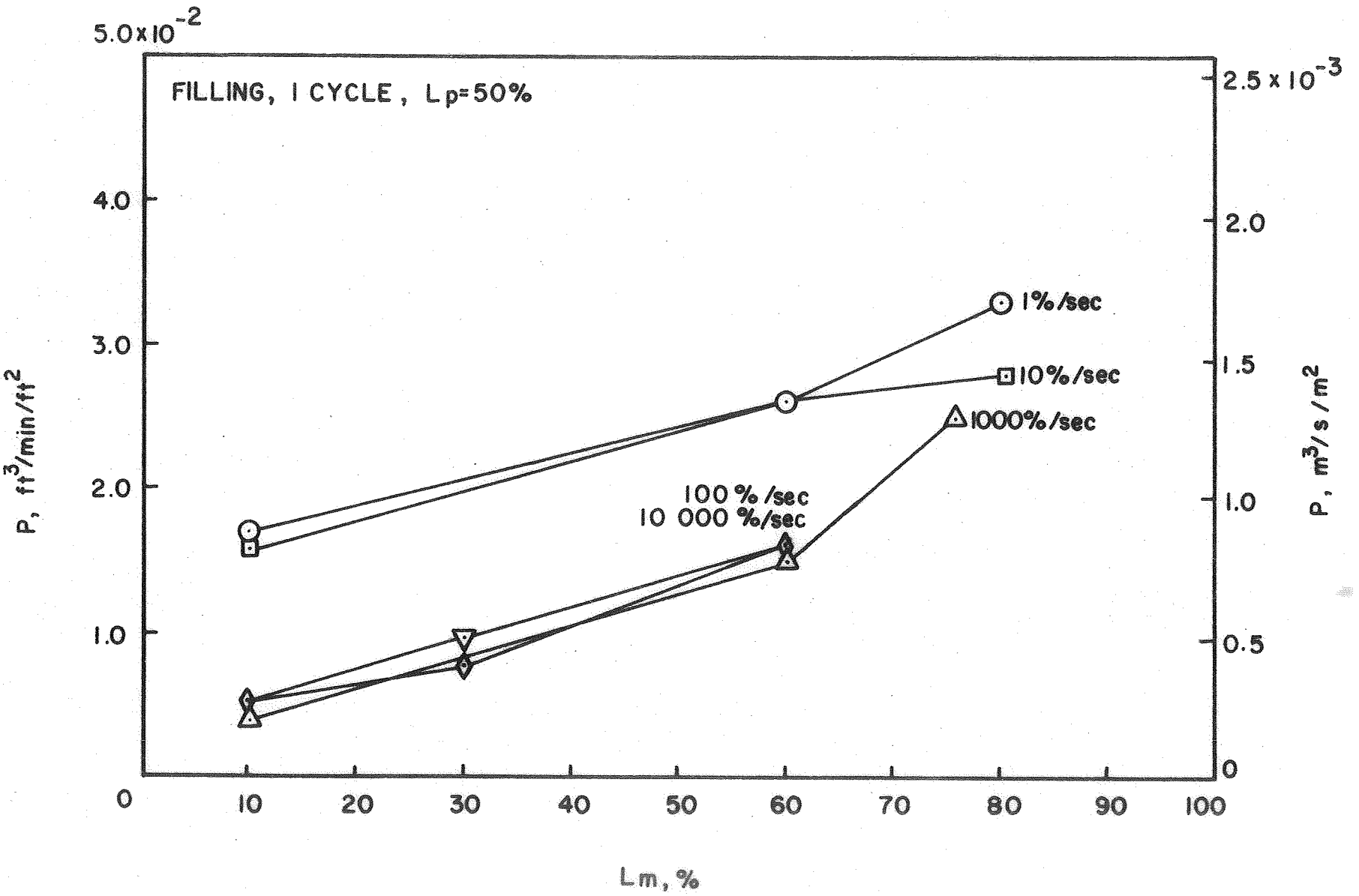

Figure 21. Variation of Air Permeability, P, with Load, Lm, for Fabric Prestressed Uniaxially at Various Strain Rates. Filling Direction, 1 Cycle of Prestress to 50% of Breaking Load

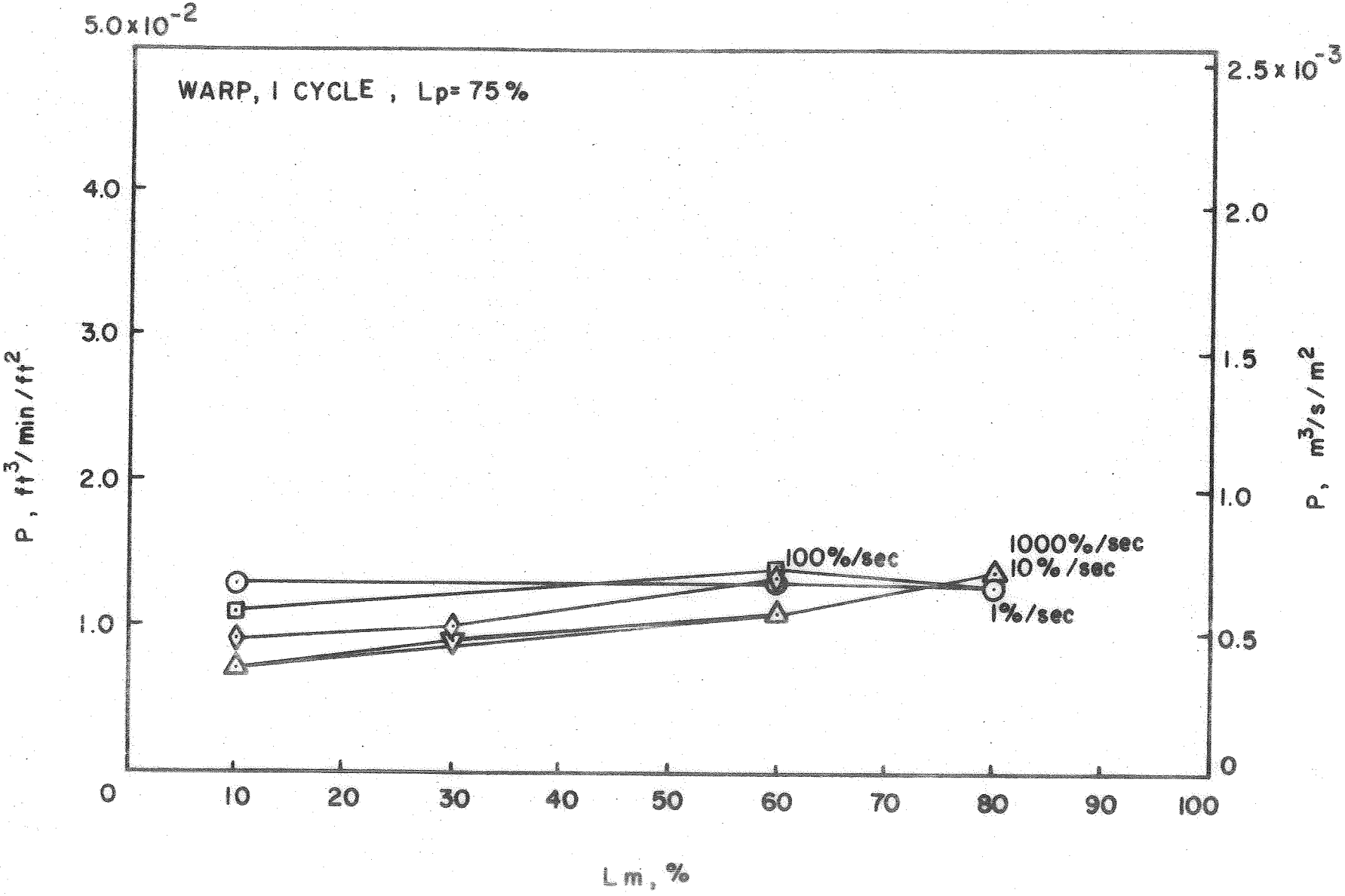

Figure 22. Variation of Air Permeability, P, with Load, Lm, for Fabric Prestressed Uniaxially at Various Strain Rates. Warp Direction, 1 Cycle of Prestress to 75% of Breaking Load

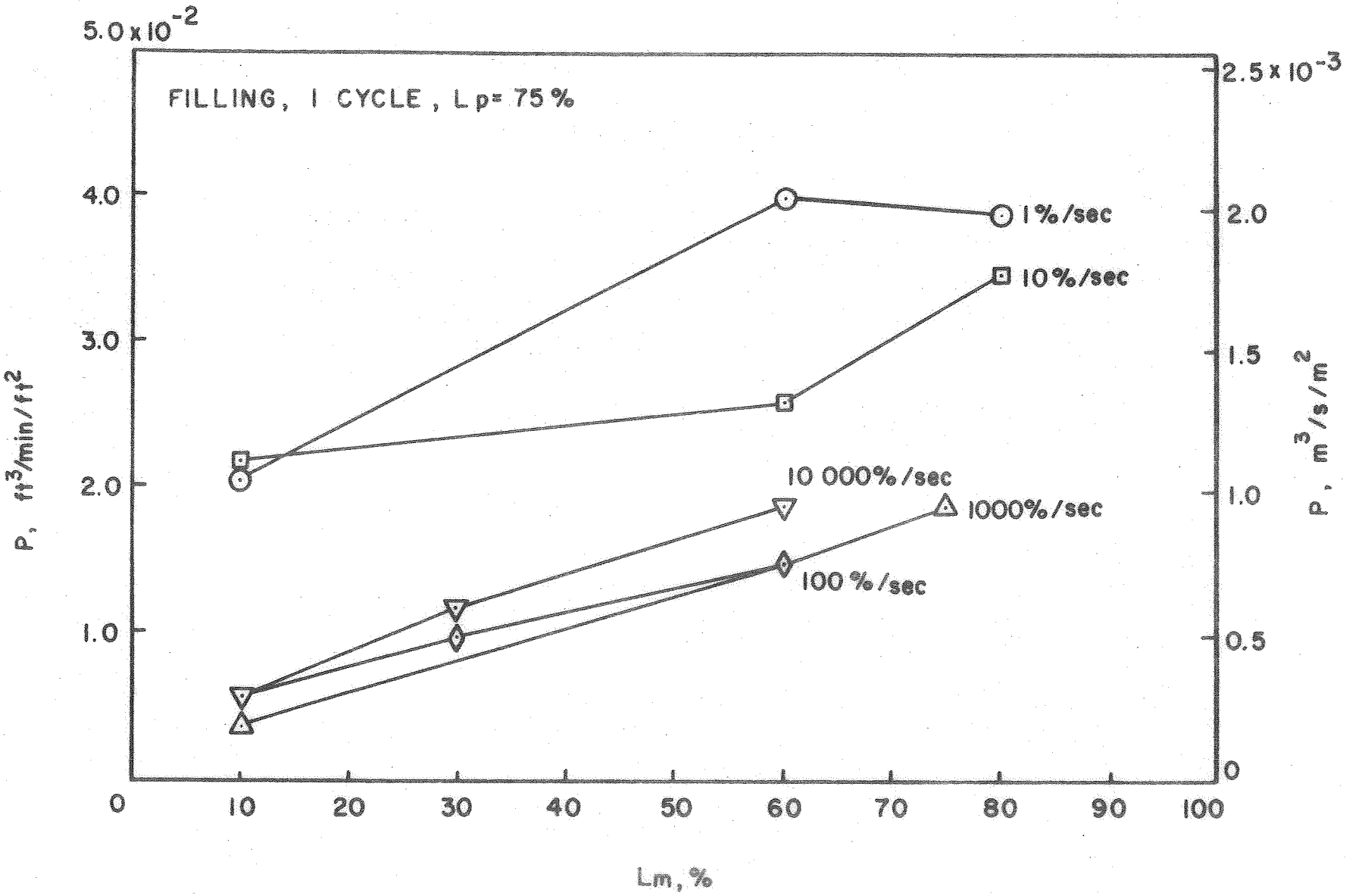

Figure 23. Variation of Air Permeability, P, with Load, Lm, for Fabric Prestressed Uniaxially at Various Strain Rates. Filling Direction, 1 Cycle of Prestress to 75% of Breaking Load

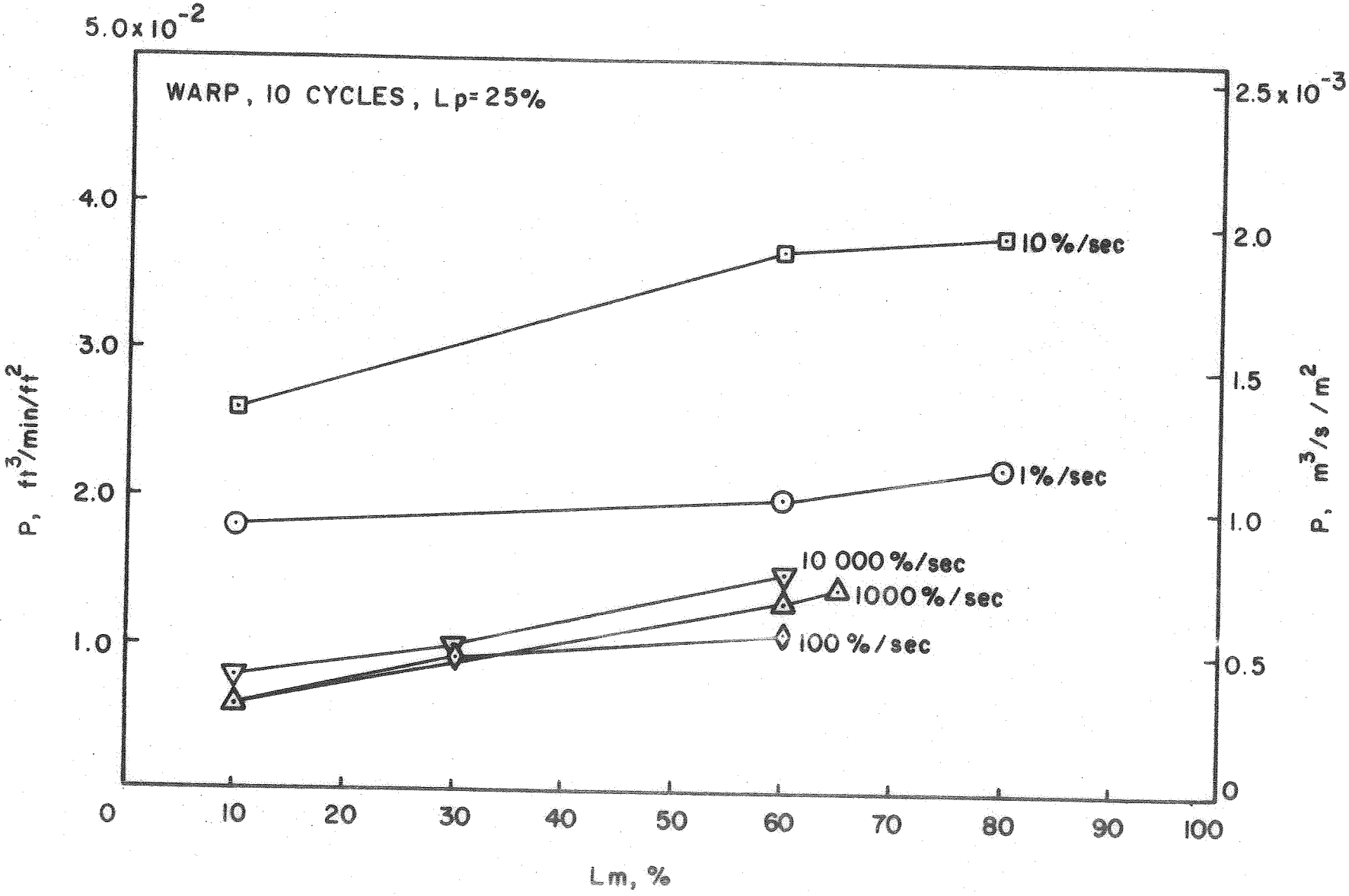

Figure 24. Variation of Air Permeability, P, with Load, Lm, for Fabric Prestressed Uniaxially at Various Strain Rates. Warp Direction, 10 Cycles of Prestress to 25% of Breaking Load

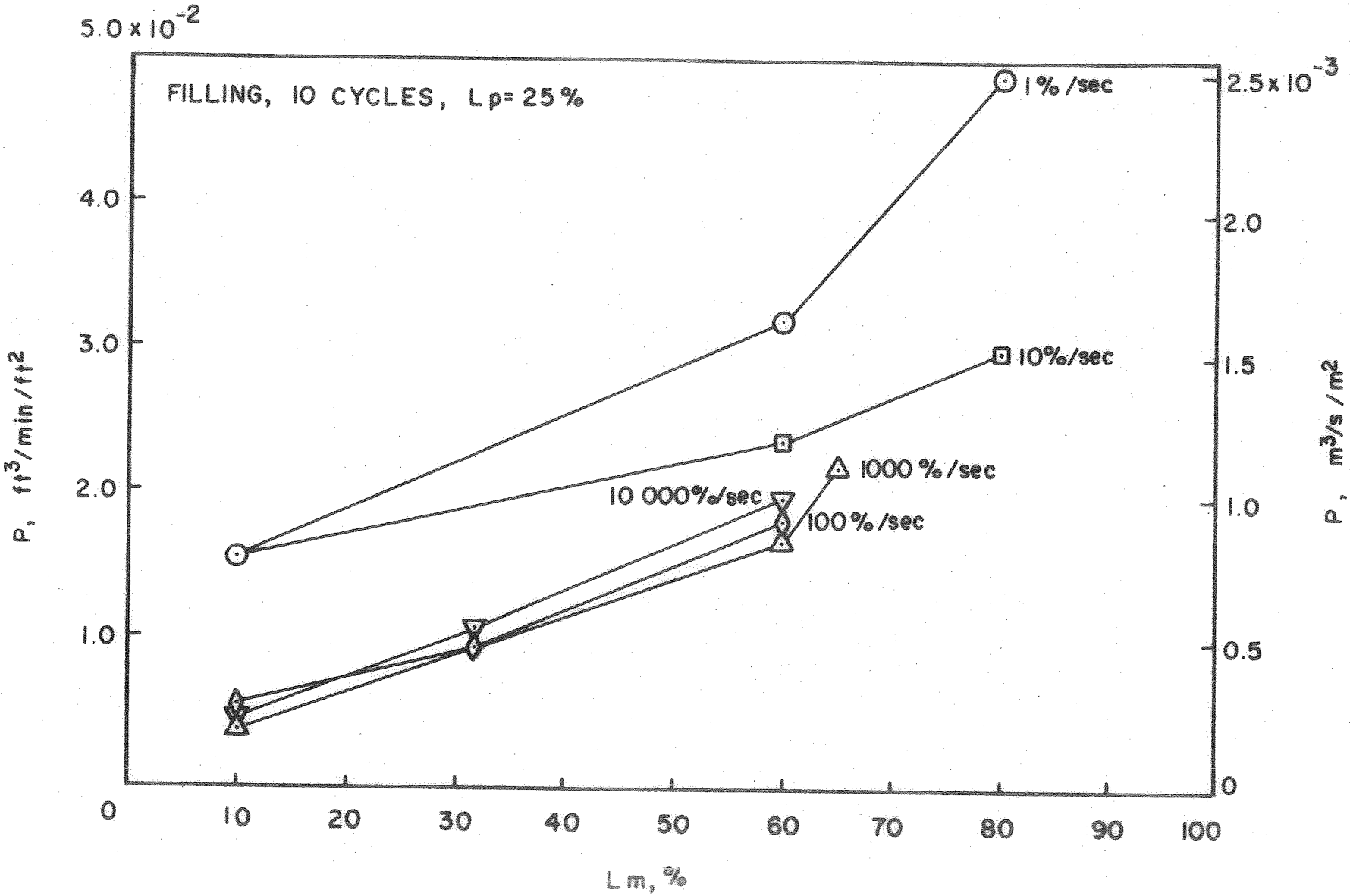

Figure 25. Variation of Air Permeability, P, with Load, Lm, for Fabric Prestressed Uniaxially at Various Strain Rates. Filling Direction, 10 Cycles of Prestress to 25% of Breaking Load

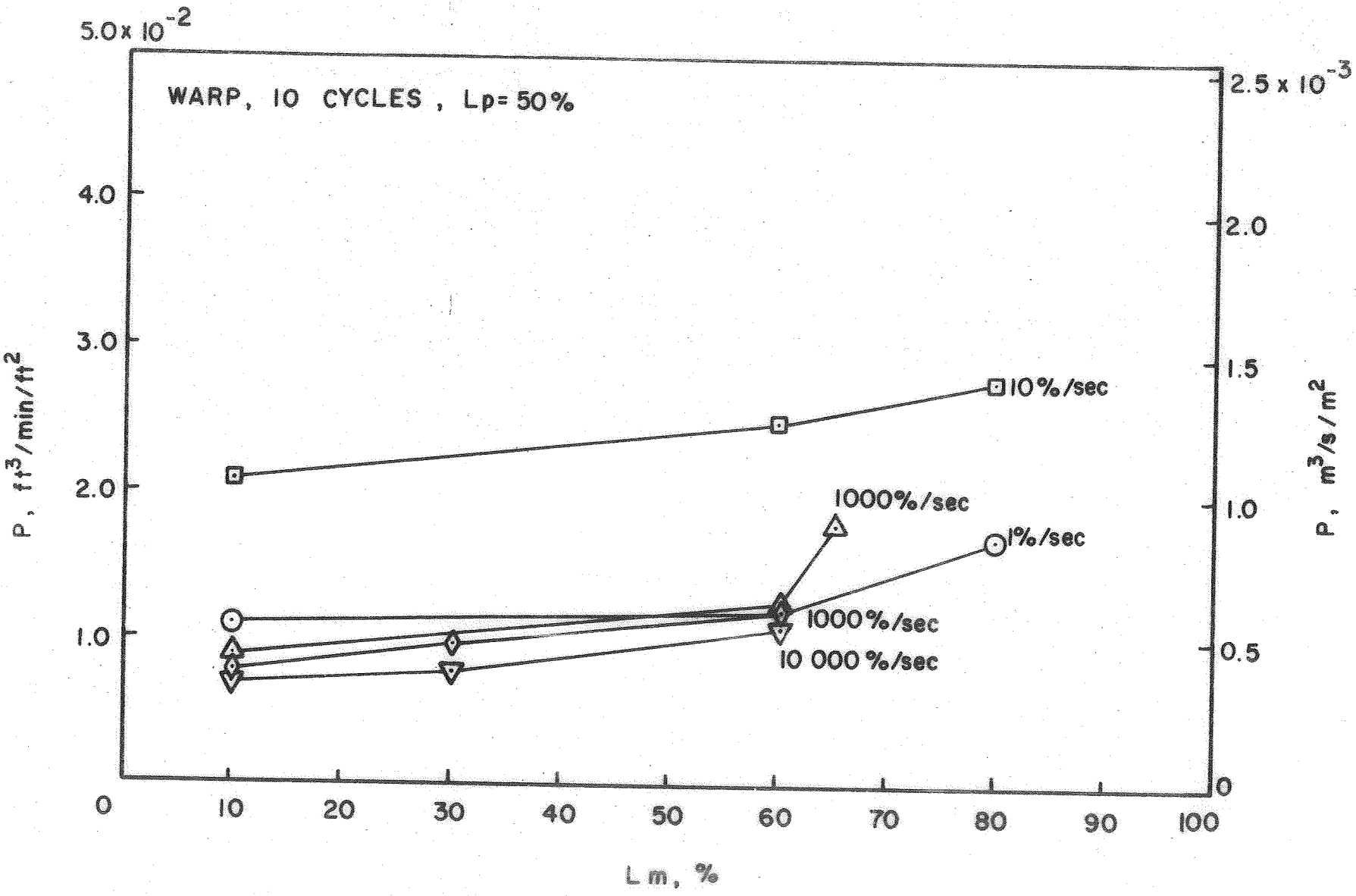

Figure 26. Variation of Air Permeability, P, with Load, Lm, for Fabric Prestressed Uniaxially at Various Strain Rates. Warp Direction, 10 Cycles of Prestress to 50% of Breaking Load

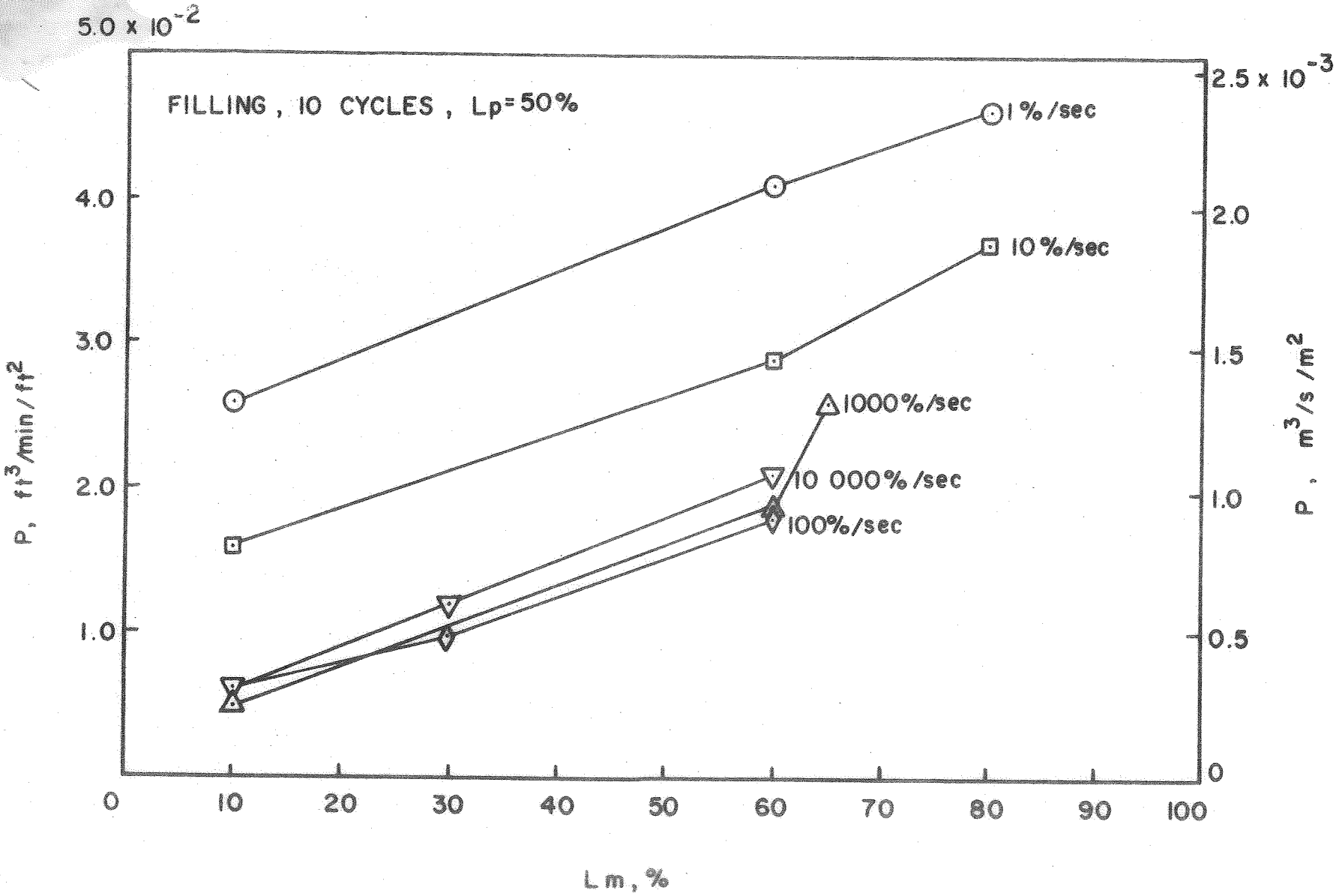

Figure 27. Variation of Air Permeability, P, with Load, Lm, for Fabric Prestressed Uniaxially at Various Strain Rates. Filling Direction, 10 Cycles of Prestress to 50% of Breaking Load

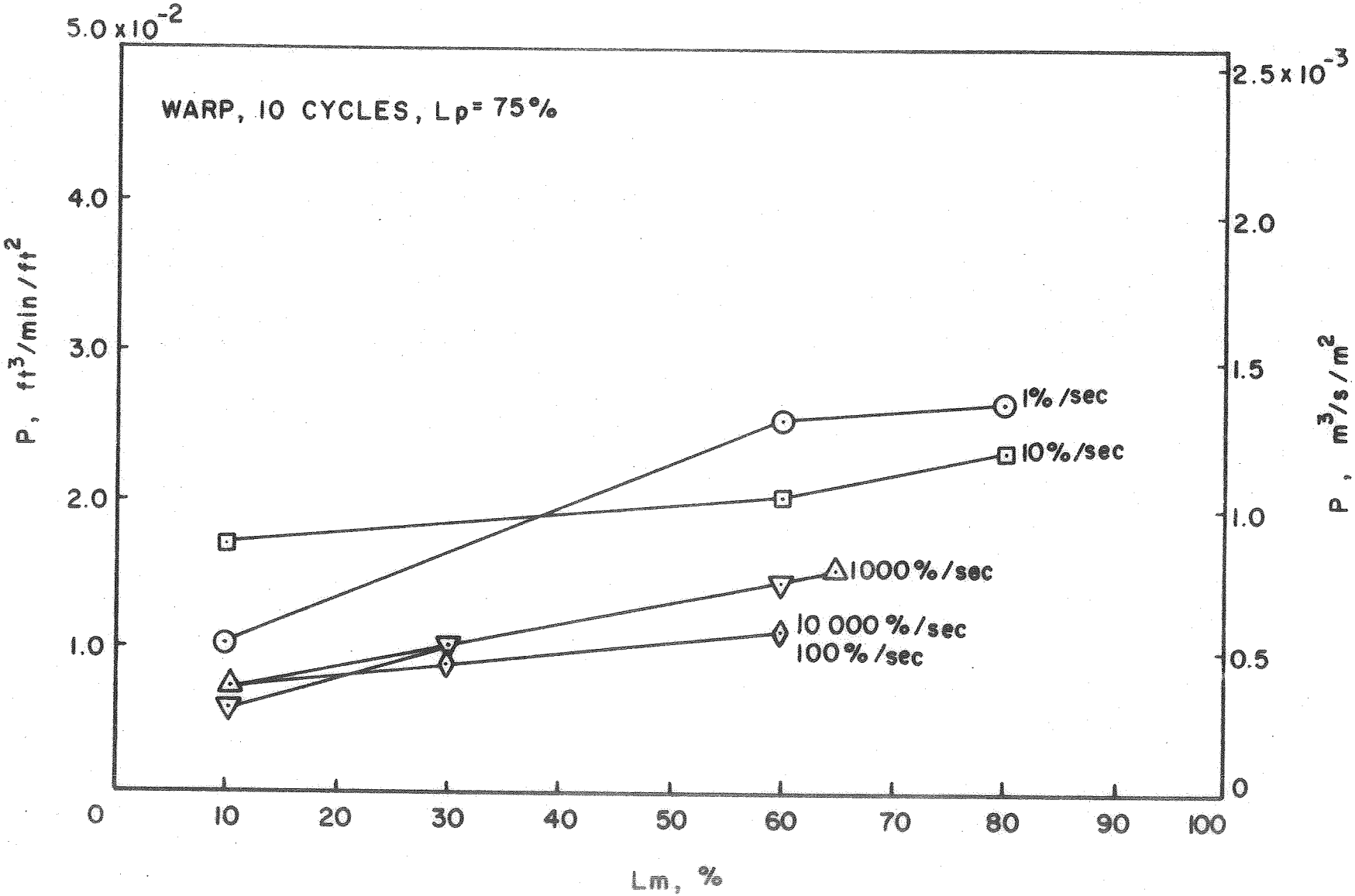

Figure 28. Variation of Air Permeability, P, with Load, Lm, for Fabric Prestressed Uniaxially at Various Strain Rates. Warp Direction, 10 Cycles of Prestress to 75% of Breaking Load

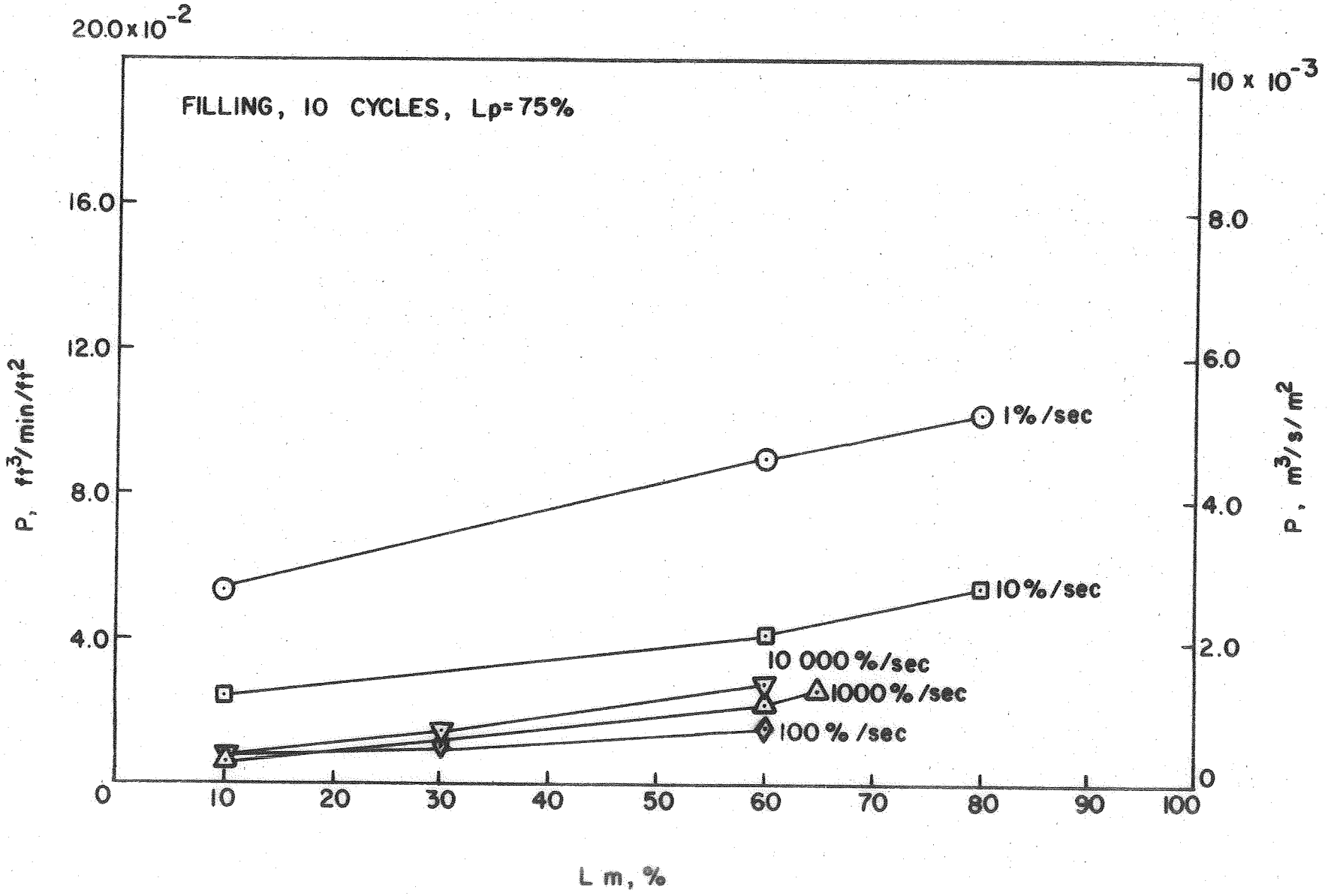

Figure 29. Variation of Air Permeability, P, with Load, Lm, for Fabric Prestressed Uniaxially at Various Strain Rates. Filling Direction, 10 Cycles of Prestress to 75% of Breaking Load

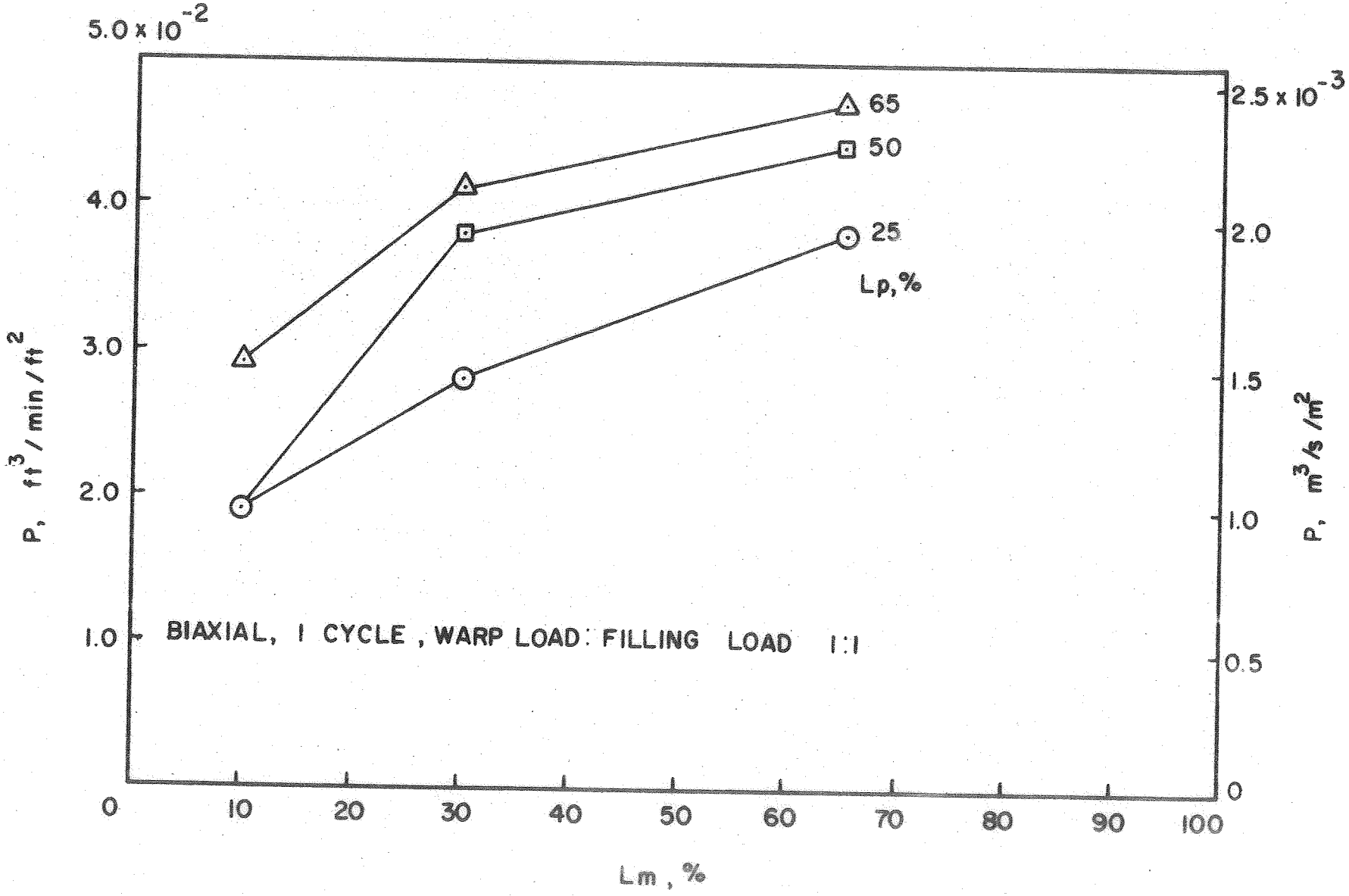

Figure 30. Variation of Air Permeability, P, with Load, Lm, for Fabric Prestressed Biaxially to Various Load Levels, Lp. 1 Cycle of Prestress, Warp Load/Filling Load 1:1

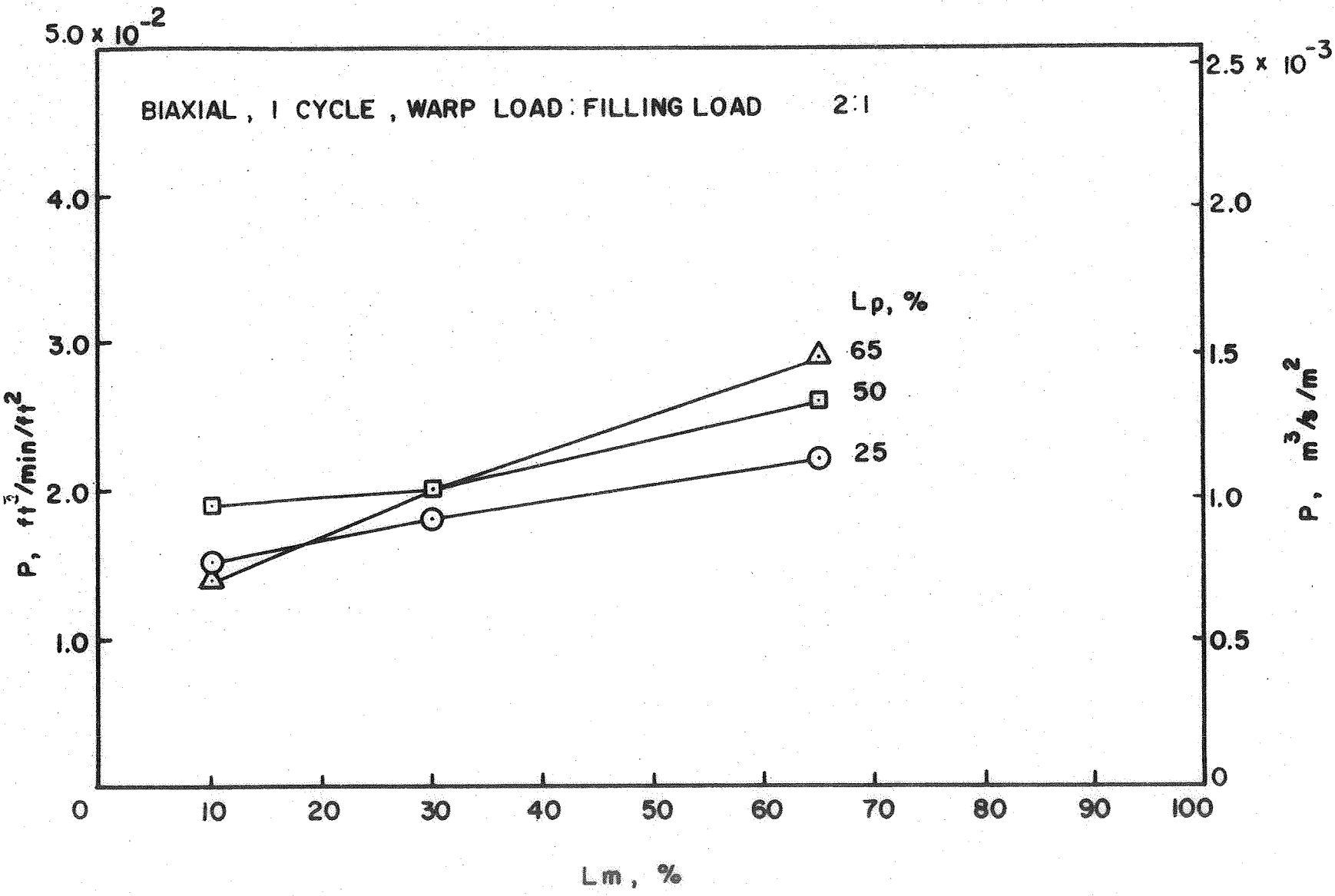

Figure 31. Variation of Air Permeability, P, with Load, Lm, for Fabric Prestressed Biaxially to Various Load Levels, Lp. 1 Cycle of Prestress, Warp Load/Filling Load 2:1

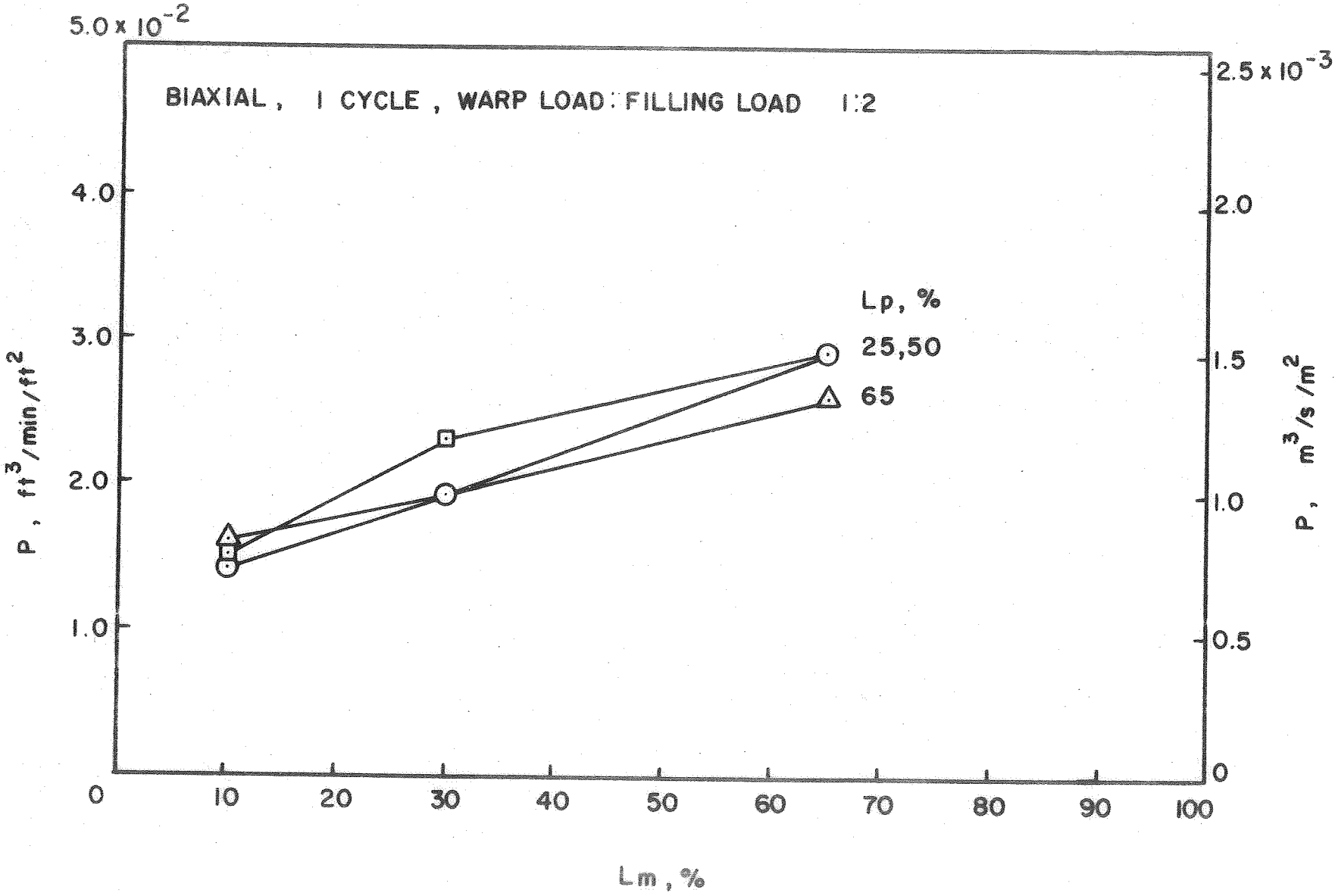

Figure 32. Variation of Air Permeability, P, with Load, Lm, for Fabric Prestressed Biaxially to Various Load Levels, Lp. 1 Cycle of Prestress, Warp Load/Filling Load 1:2

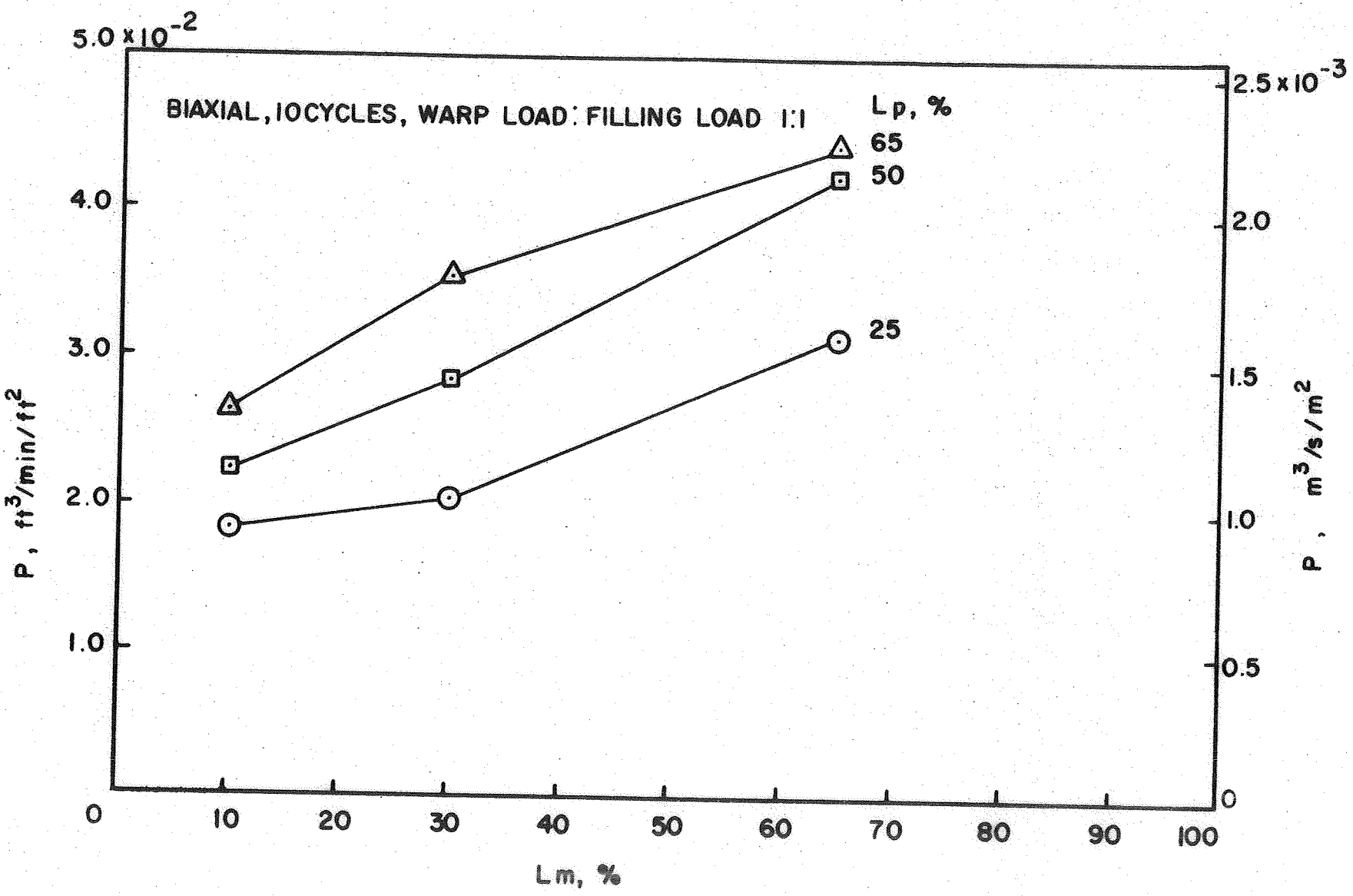

Figure 33. Variation of Air Permeability, P, with Load, Lm, for Fabric Prestressed Biaxially to Various Load Levels, Lp. 10 Cycles of Prestress, Warp Load/Filling Load 1:1

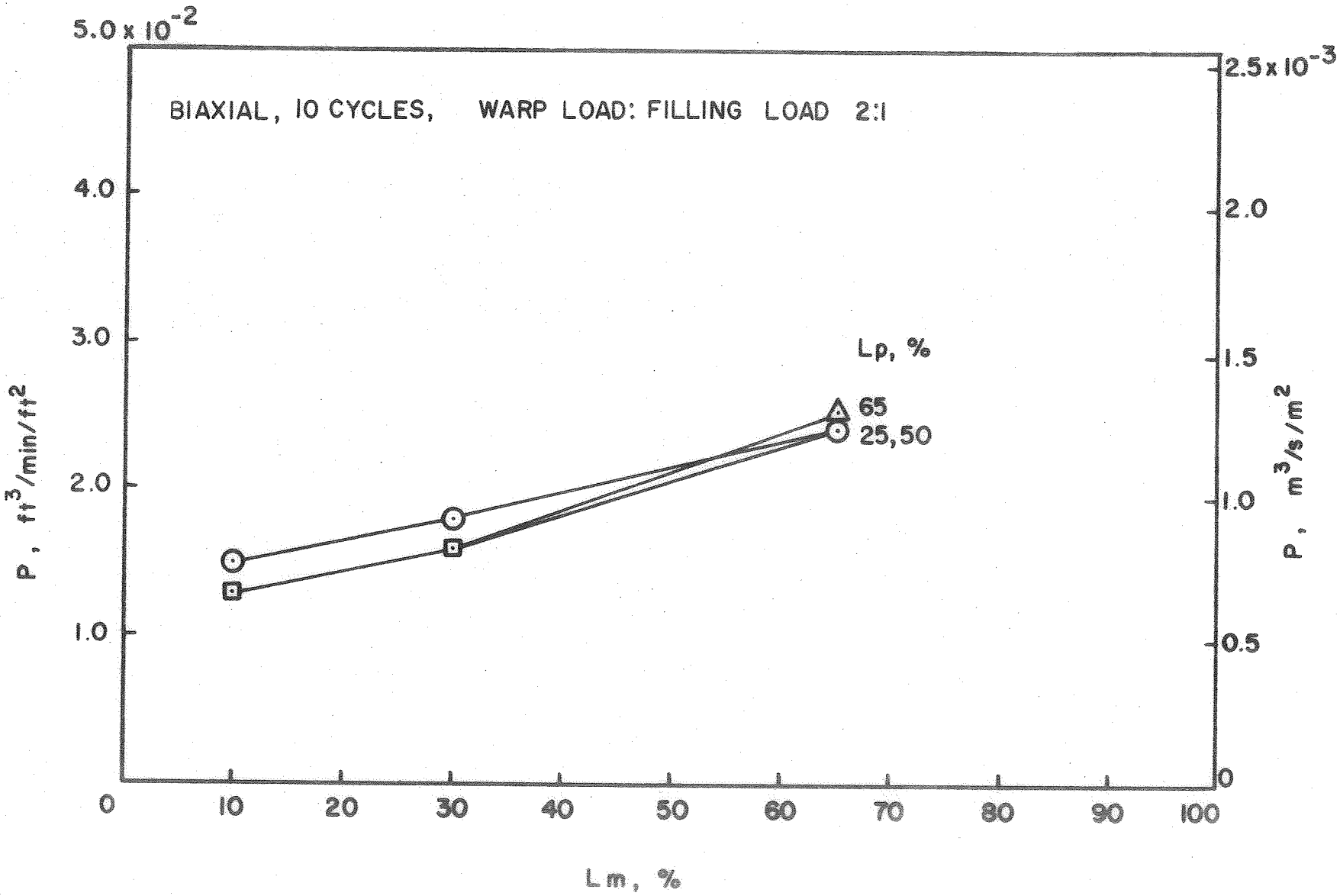

Figure 34. Variation of Air Permeability, P, with Load, Lm, for Fabric Prestressed Biaxially to Various Load Levels, Lp. 10 Cycles of Prestress, Warp Load/Filling Load 2:1

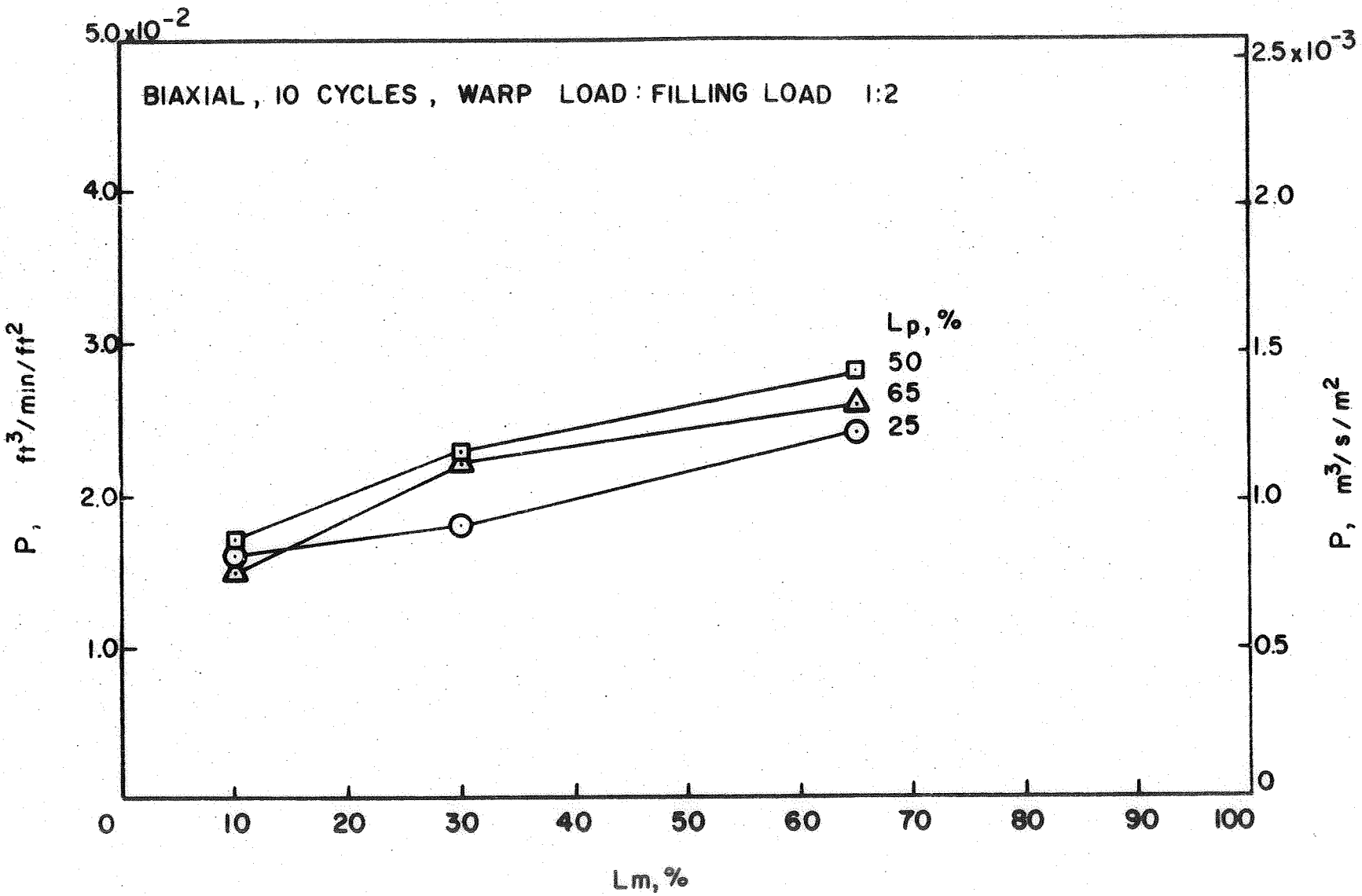

Figure 35. Variation of Air Permeability, P, with Load, Lm, for Fabric Prestressed Biaxially to Various Load Levels, Lp. 10 Cycles of Prestress, Warp Load/Filling Load 1:2